Neuron, Vol. 36, 1127–1143, December 19, 2002, Copyright ©2002 by Cell Press

Optimizing Synaptic Architecture and Efficiency for High-Frequency Transmission

Holger Taschenberger,[1] Ricardo M. Leão,[1] Kevin C. Rowland,[2] George A. Spirou,[2] and Henrique von Gersdorff[1,3]
[1]The Vollum Institute
Oregon Health and Science University
3181 SW Sam Jackson Park Road
Portland, Oregon 97201
[2]Sensory Neuroscience Research Center
Department of Otolaryngology
Department of Physiology
West Virginia University School of Medicine
Health Sciences Center
PO Box 9303
Morgantown, West Virginia 26506

Summary

Bursts of neuronal activity are transmitted more effectively as synapses mature. However, the mechanisms that control synaptic efficiency during development are poorly understood. Here, we study postnatal changes in synaptic ultrastructure and exocytosis in a calyx-type nerve terminal. Vesicle pool size, exocytotic efficiency (amount of exocytosis per Ca influx), Ca current facilitation, and the number of active zones (AZs) increased with age, whereas AZ area, number of docked vesicles per AZ, and release probability decreased with age. These changes led to AZs that are less prone to multivesicular release, resulting in reduced AMPA receptor saturation and desensitization. A greater multiplicity of small AZs with few docked vesicles, a larger pool of releasable vesicles, and a higher efficiency of release thus promote prolonged high-frequency firing in mature synapses.

Introduction

Synapses exhibit wide morphological diversity, and newly formed synaptic contacts often have distinct functional properties from those of mature synapses (Carr et al., 2001; Craig and Lichtman, 2001). Postsynaptic developmental changes are relatively well documented, but changes in presynaptic machinery are less understood, in part because of the inaccessibility of most nerve terminals to direct patch-clamp recording. Several studies of CNS synapses have noted little developmental change in the size of active zones (AZs) and postsynaptic densities (PSD), although a 4-fold increase in number of vesicles per bouton was reported during the first postnatal month in visual cortex (Blue and Parnavelas, 1983; Vaughn, 1989). However, important determinants of presynaptic release capacity, such as the number of docked vesicles at individual AZs (Harris and Sultan, 1995; Schikorski and Stevens, 1997), the multiplicity of AZs (Hsia et al., 1998), and the efficiency of exocytosis are, for example, largely unexplored at most synapses developing in vivo.

The calyx of Held, a giant glutamatergic terminal of the auditory brainstem, and its postsynaptic partner, the principal cell of the medial nucleus of the trapezoid body (MNTB), can be studied directly via whole-cell patch-clamp recordings (Forsythe, 1994; Borst et al., 1995). However, it is not known how the synaptic ultrastructure changes during development, and basic functional properties, such as the pool size of readily releasable vesicles, have proven difficult to determine (Schneggenburger et al., 1999; Sakaba and Neher, 2001; Sun and Wu, 2001). It has been proposed that the vesicle pool size increases during development (Taschenberger and von Gersdorff, 2000; Iwasaki and Takahashi, 2001). However, the methods used (recordings of AMPA-R-mediated EPSCs) are prone to uncertainties due to receptor saturation and desensitization (Trussell et al., 1993; Chen et al., 2002; Scheuss et al., 2002). In addition, there is considerable debate over the degree of changes in release probability during development (Chuhma and Ohmori, 1998; Iwasaki and Takahashi, 2001; Dobrunz, 2002), as well as the underlying mechanisms of developmental changes in short-term synaptic plasticity (Wu and Oertel, 1987).

Here, we report how presynaptic ultrastructure and functional properties of the calyx of Held change during development to produce an exceptionally fast and efficient excitatory synapse. We combined electron microscopy, presynaptic membrane capacitance (C_m) measurements, and EPSC recordings to study developmental alterations from postnatal day 5 (P5, just after calyx formation; Kandler and Friauf, 1993) to P14, just after the onset of hearing. Recently, C_m measurements have been performed on the calyx of Held of P8–P10 rats, and it was shown that C_m jumps evoked by step depolarizations are well correlated with glutamate release (Sun and Wu, 2001). Here, we extend such measurements to immature (P5–P7) and mature (P12–P14) calyces to compare their exocytotic capacity and efficiency. We apply novel and standard compounds that reduce AMPA receptor (AMPA-R) saturation and desensitization at distinct receptor subtypes to compare the efficacy of synaptically released glutamate in generating EPSCs. The mean probability for vesicle release (P_{ves}) was low for immature synapses (0.28), and further decreased during maturation (0.13). By contrast, quantal size increased from P5 to P14 (Bellingham et al., 1998). Finally, we find that the AZs of mature terminals are smaller than immature AZs and have a correspondingly lower number of docked vesicles. The faster presynaptic action potentials of mature synapses are thus less likely to trigger fusion of multiple vesicles at individual AZs (Oertner et al., 2002). This results in a presumably smaller and less prolonged glutamate transient in the synaptic cleft of mature synapses and consequently causes a smaller degree of saturation and desensitization of postsynaptic AMPA-R (Brenowitz and Trussell, 2001; Wadiche and Jahr, 2001; Joshi and Wang, 2002). Together with a larger pool of readily releasable vesicles, this prevents

[3]Correspondence: vongersd@ohsu.edu

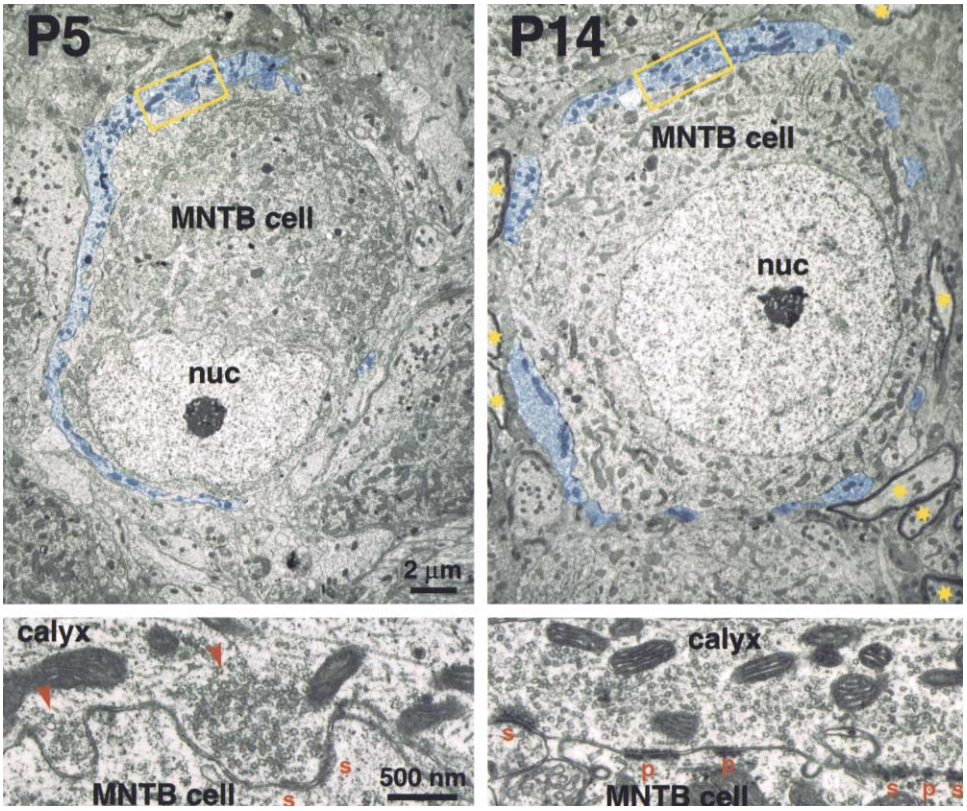

Figure 1. Ultrastructure of Calyces of Held and Their Postsynaptic Targets at Postnatal Days 5 and 14 (P5 and P14)

The calyces in contact with the MNTB cells in the center of each top image are colored blue. P5: the cup-shaped calyx appears as a continuous structure in crosssection. The yellow boxed area is enlarged in the bottom image and reveals clusters of vesicles (red arrowheads), one of which is located nearby active zones (AZs), the presynaptic component of synapses (s), in the same tissue section. Aside from the vesicle clusters near the membrane, the cytoplasm of the P5 calyx is relatively devoid of vesicles. P14: the cell body and nucleus (nuc) are rounder and larger than at P5, and myelinated axons are evident (yellow asterisks). The boxed area is enlarged in the bottom image, revealing that synaptic vesicles are distributed more evenly throughout the P14 calyx but not in association with puncta adhaerentia (p).

severe synaptic depression and enables mature synapses to follow high-frequency bursts of presynaptic activity.

Results

Development of Calyx Ultrastructure

We performed a partial serial EM reconstruction of four calyces (5% of each calyx) at both postnatal days P5 and P14 (Figure 1). At both ages the MNTB is recognizable as a cluster of cells located medially in the superior olivary complex. The MNTB principal cells appear ovoid in cross section and have greater surface area at P14 than at P5 (1058 $\pm$ 86 μm^2 versus 768 $\pm$ 51 μm^2; $n = 10$, $p < 0.01$, see Experimental Procedures). At P5, calyceal nerve terminals are cup shaped (Morest, 1968) and, in ultrathin sections, appear as a single process enveloping much of the MNTB cell surface (blue pastel in Figure 1). In single sections at P14, pieces of the calyx appear discontinuous as the structure matures into a more complex form of stalks and small branches, called necks, that terminate in bulbous processes called swellings (Rowland et al., 2000). Isolated profiles that belong to calyceal appendages can be clearly distinguished from noncalyceal boutons because the latter have pleomorphic vesicles and less pronounced PSDs (Jean-Baptiste and Morest, 1975; Lenn and Reese, 1966). These images reveal that a large portion of the MNTB cell is contacted by the calyx (P5, 62.6% $\pm$ 9.4% [SD]; P14, 55.8% $\pm$ 12.9%). At both ages synapses and puncta adhaerentia, attachment points between cells, are located along the entire length of the calyx where it is apposed to the MNTB neuron. In P5 animals, synaptic vesicles tend to cluster exclusively around AZs. At P14, vesicles often fill the entire volume of a calyceal swelling (Figure 1, bottom images). Myelinated axons are absent at P5 but are prominent at P14.

Figure 2A shows two AZs in each micrograph of a P5 calyx; one AZ contained multiple vesicles docked to the presynaptic membrane (colored green). AZs and PSDs from P14 calyces tended to be smaller than in the younger animals (Figure 2A, right column). The average PSD surface area decreased by over one-third between P5 (84,924 nm^2) and P14 (54,812 nm^2). At both ages there was a monotonic relationship between PSD surface area and the number of docked vesicles, fit by lines with similar slopes (Figure 2B). The number of docked vesicles per AZ also decreased by nearly one-half between

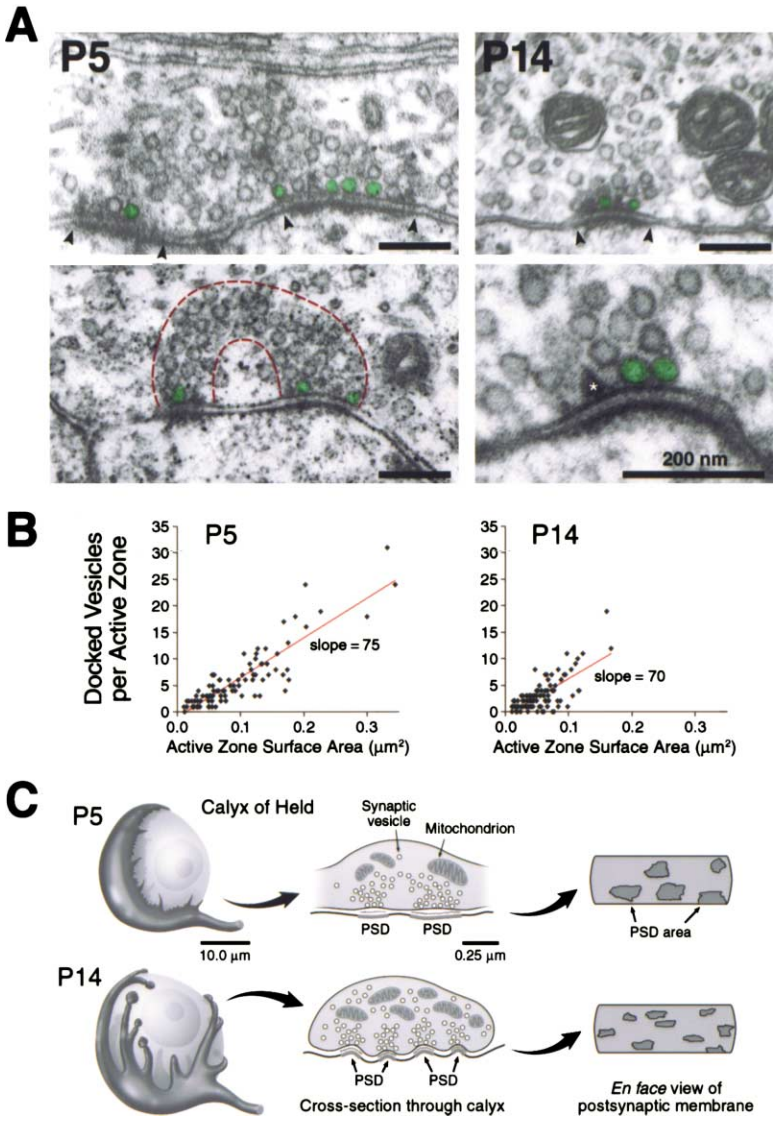

Figure 2. Postsynaptic Density (PSD) Size Changes during Development

(A) Association of vesicles with active zones at P5 (left) and P14 (right). Docked vesicles, defined as those in contact with the presynaptic membrane, are colored light green. P5: PSDs tend to be larger than at P14 (limits marked by arrowheads in top row) and, when located nearby one another, can be connected by an arc of streaming synaptic vesicles (red dashed lines, bottom left). P14: high magnification in bottom right image reveals widening of synaptic cleft and the presence of a presynaptic pyramidal dense projection (asterisk), a characteristic of synapses at both P5 and P14. Scale bar in all panels equals 200 nm.

(B) Graphs reveal a correlation between PSD size (or AZ surface area) and the number of docked vesicles at AZs in both P5 and P14. Small PSDs are found at both ages, but an additional population of large PSDs is found in the young animals. At P14 several AZs had no docked vesicles although they had associated vesicle clusters.

(C) Schematic depicts maturation of calyx from a cup shape to a highly branched structure with fenestrations, and a hypothesized breakup of large PSDs into smaller PSDs during development. The fenestrations in the mature calyx morphology could help released glutamate diffuse more quickly out of the synaptic cleft. This structural rearrangement may also avoid depletion of external Ca^{2+} ions within the cleft during high-frequency firing.

P5 (5.7 ± 1.7) and P14 (3.3 ± 1.2 [SD], Table 1). This age-related difference was due to the absence of large PSDs in P14 calyces coupled with a population of AZs having no docked vesicles. At both ages the percent of calyx surface apposed to MNTB cell surface and occupied by AZs was similar (P5, 5.23 ± 0.72 [SD]; P14, 6.07 ± 1.99), but the total PSD surface area per calyx was larger for P14 than P5 animals because MNTB cells were larger in older animals. Because of the similar fraction of calyx surface devoted to PSDs at both ages (about 5%) and the smaller size of PSDs at P14, the total number of PSDs and AZs per calyx more than doubles from P5 (~303) to P14 (~678). However, because P5 synapses have on average nearly twice as many docked vesicles per AZ, P14 calyces are estimated to contain only about 25% more docked vesicles per calyx than P5 calyces (2117 ± 368 versus 1697 ± 218; Table 1). The average number of puncta adhaerentia (p; Figure 1) per calyx was 765 ± 118 for P5 (individual estimates for the four calyces: 908, 686, 652, 813) and 1447 ± 369 for P14 (individual estimates: 1694, 1589, 1606, 898).

We noticed that vesicle clusters often appeared to "stream" from one active zone to another in the P5 calyces (Figure 2A, bottom left, red dashed line) but were not observed to do so in P14 calyces. We speculate that this vesicle arrangement may be a stage in the splitting of a large AZ into two smaller AZs. The average synaptic vesicle outer diameter was 46.1 ± 5.9 nm (P5) and 42.3 ± 5.5 nm (P14; n = 450 vesicles for both ages). However, this difference was not significant. A similar value (48 nm) was reported by Sätzler et al. (2002) for a P9 rat calyx. Taking into account a ~12% decrease in the diameter of glutamatergic synaptic vesicles in the cochlear nucleus caused by tissue fixation (Tatsuoka and Reese, 1989), we estimate mean vesicle diameters of 47 nm (P14) to 51 nm (P5). The vesicle volume is thus much larger than at other CNS regions (30–35 nm diameters; Schikorski and Stevens, 1997), perhaps because a larger bolus of glutamate is needed to activate

Table 1. Postsynaptic Density Size and Number of Docked Vesicles

		Average PSD Surface Area (nm^2)	Estimated Number of AZs/Calyx	Average Number of Docked Vesicles/AZ	Estimated Number of Docked Vesicles/Calyx
P5	calyx 1 (25)	95,311	318	7.2	2290
	calyx 2 (27)	98,809	239	7.2	1721
	calyx 3 (19)	80,672	295	4.3	1267
	calyx 4 (20)	64,903	360	4.2	1510
	mean	84,924 ± 7,744	303 ± 25	5.7 ± 0.9	1697 ± 218
P14	calyx 1 (14)	70,538	510	5.1	2600
	calyx 2 (33)	47,155	1106	2.6	2875
	calyx 3 (36)	48,811	635	2.6	1651
	calyx 4 (23)	52,744	462	2.9	1341
	mean	54,812 ± 5,371	678 ± 147	3.3 ± 0.6	2117 ± 368
		$p = 0.043$[a]	$p = 0.020$[a]	$p = 0.079$	

Due to the time-intensive process of serial EM reconstruction, only a small number of samples were available per age. Number of active zones measured per calyx given in parentheses. PSDs and AZs show some heterogeneity in size among the different calyces and within a given calyx. Statistical comparisons were made using Mann-Whitney U test.
[a] $p < 0.05$ (or <5%)

the low-affinity AMPA-R. Figure 2C schematizes the main developmental changes in the architecture of the calyx of Held, including our observation that more of the PSDs were curved at P14 (75%; n = 79) than at P5 (47%; n = 55).

Lack of AP Broadening and I_{Ca} Inactivation during Short Trains

Synaptic depression in immature and mature calyx of Held synapses is remarkably different (Taschenberger and von Gersdorff, 2000). Here, we explore the functional synaptic properties that may underlie such differences and relate them to the above morphological findings. Presynaptic action potentials (APs) can undergo significant changes during long stimulus trains (Geiger and Jonas, 2000; Martin and Pilar, 1964). Previous recordings in the rat calyx of Held (P8–P10) indicated some AP broadening during prolonged trains (Borst and Sakmann, 1999). We therefore asked if the different capabilities of immature and mature synapses to follow high-frequency inputs could, in part, be related to differential changes in presynaptic AP waveform. For both P5–P7 and P12–P14 calyces, presynaptic APs could be reliably elicited by afferent fiber stimulation at frequencies of up to 100 Hz. In immature calyces, higher frequencies typically resulted in a number of failures (2–3 out of 15 stimuli for 300 Hz; data not shown) and were therefore not used in this study.

Figure 3A illustrates 100 Hz trains of presynaptic APs evoked by afferent fiber stimulation. The first and last (15^{th}) AP in the train are superimposed at an expanded time scale. As previously reported (Taschenberger and von Gersdorff, 2000), the width of calyceal APs greatly decreased as terminals matured. However, during short trains only a minor broadening of APs was detected in both age groups. From the first to the last AP, the half-width increased on average by less than 5% in P5–P7 terminals (from 457 ± 30 μs to 479 ± 31 μs, n = 9) and by less than 2% in P12–P14 terminals (from 208 ± 22 μs to 211 ± 22 μs, n = 4; Figure 3A, right). We therefore conclude that calyceal APs are resistant to broadening for short stimulus trains.

Presynaptic Ca currents (I_{Ca}) in the calyx of Held inactivate during long-lasting tetanic stimulation (e.g., 1500 stimuli at 100 Hz; Forsythe et al., 1998), and this inactivation contributes to posttetanic depression of EPSCs. However, as illustrated in Figure 3B, no significant decrease in amplitude of I_{Ca} was seen during short 100 Hz trains of 15 depolarizing steps from a holding potential (V_h) of −80 mV to 0 mV (1 ms duration). In fact, facilitation was frequently observed in both immature and mature calyces for the first three depolarizations in the train (Borst and Sakmann, 1998b; Cuttle et al., 1998). Mean values for the Ca charge (Q_{Ca}) during the first and the last I_{Ca} in the 15 stimuli train were 1.6 ± 0.2 pC (P5–P7) and 1.8 ± 0.2 pC (n = 8; P12–P14) for the first stimulus and 1.7 ± 0.3 pC (P5–P7) and 2.3 ± 0.4 pC (n = 3; P12–P14) for the last stimulus. Thus, Q_{Ca} was on average slightly larger and exhibited stronger facilitation in mature terminals.

In Figure 3C, I_{Ca} elicited in a P7 calyx by a 1 ms depolarization (0 mV) and by an immature AP waveform (P6) are superimposed for comparison. On average, Q_{Ca} produced by both voltage commands was similar at this age (Table 2). Thus, 1 ms pulses to 0 mV approximated well the physiological AP depolarization in immature terminals. The large membrane capacitance of the calyx (see below), however, prevented use of the fast, mature APs as voltage commands to reliably measure AP-driven I_{Ca} in P12–P14 terminals with single electrode voltage-clamp (Borst and Sakmann, 1996). On the other hand, it is likely that at this age, the Q_{Ca} produced by 1 ms depolarizations to 0 mV is larger than AP-driven Q_{Ca}, taking into account that mature APs are shortened by >50%. In P8–P10 synapses, 1 ms depolarizations to +7 mV are equivalent to AP-driven Q_{Ca} (Sun et al., 2002). To more realistically mimic AP-driven Ca influx in mature terminals, we therefore resorted to stronger depolarizations (+40 mV, the peak of the AP; Figure 3D) in some experiments (Sakaba and Neher, 2001). This protocol resulted in smaller Q_{Ca} than depolarizations to 0 mV (Table 2), and we will refer to the two different stimuli (1 ms, 0 mV for immature and 1 ms, +40 mV for mature terminals) as AP-like depolarizations.

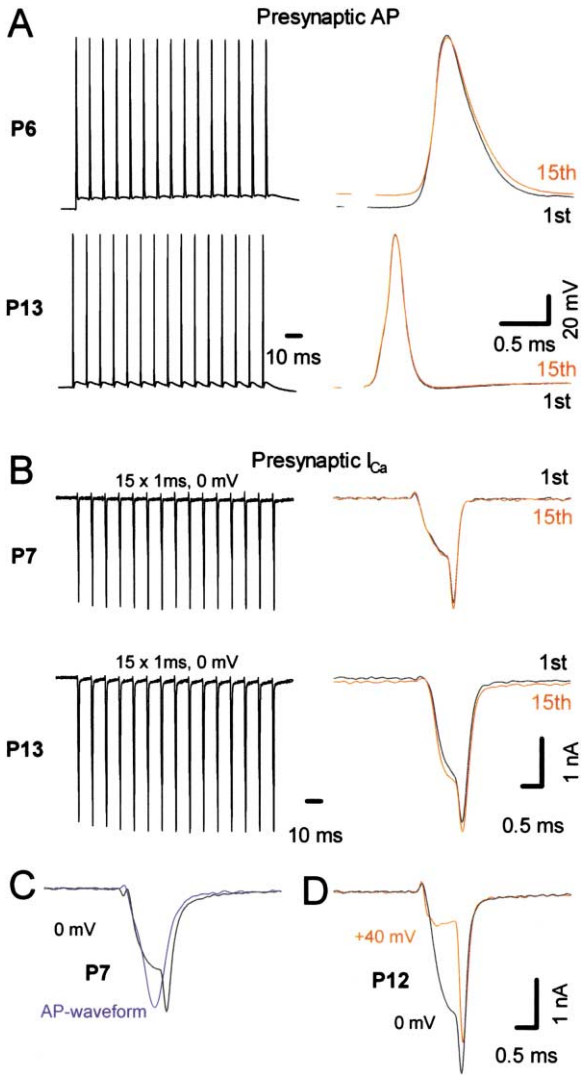

Figure 3. Presynaptic AP Waveform and Ca Influx during Short 100 Hz Stimulus Trains

(A) Left, trains of 15 presynaptic APs evoked by afferent fiber stimulation in P6 (top) and P13 (bottom) brainstem slices recorded at room temperature. Right, first and last APs in the train superimposed at higher time resolution. The halfwidth of calyceal APs was significantly shorter in mature synapses. However, at both developmental stages, amplitudes and halfwidth of the APs were stable throughout the train.

(B) Left, presynaptic Ca influx during 100 Hz trains of AP-like depolarizations. I_{Ca} was elicited using 15 depolarizing steps from $V_h = -80$ mV to 0 mV (1 ms duration) in a P7 (top) and a P13 (bottom) calyx. A small facilitation of the presynaptic I_{Ca} was observed at both ages. Right, first and last I_{Ca} in the train superimposed at higher time resolution.

(C) Comparison of I_{Ca} evoked by a 1 ms step depolarization to 0 mV (black) with AP waveform-driven Ca influx (blue) recorded in a P7 terminal. The AP waveform used as the voltage command was obtained from an afferent fiber stimulation-evoked AP recorded in current-clamp in a P6 terminal.

(D) Comparison of I_{Ca} elicited by 1 ms step depolarizations to 0 mV (black) and to +40 mV (red) in a P12 terminal. The latter depolarizations produced smaller I_{Ca} and a brief tail current that more closely resemble Ca influx elicited by the shortened APs at this age.

Glutamate Release Estimated by C_m

Membrane capacitance (C_m) measurements estimate glutamate release in a manner independent of AMPA-R (Sun and Wu, 2001). However, considering the possibility that measured changes in C_m (ΔC_m) were affected by differences in passive membrane properties or access resistance, we routinely analyzed capacitive current transients evoked during brief hyperpolarizations from V_h (−80 mV) to −90 mV (Figure 4A). Average values for C_m (obtained from integrating the charging current), membrane resistance (R_m), and fast and slow time constants (obtained from fitting a double exponential function to the current transient) were similar in P5–P7 and P12–P14 calyces (Table 2). In both age groups, the fast component, which is likely to represent the capacitance of the terminal, accounted for ≥70% of the current amplitude. In a small subset of the cells (n = 3 for P5–P7 and n = 4 for P12–P14 terminals), the capacitive transients were well fit by single exponentials, probably indicating calyces with short axon stumps (Borst and Sakmann, 1998a). The capacitance "seen" by the lock-in amplifier may reflect only the calyx surface area without the associated axon because it was considerably smaller than the values obtained from integrating the charging transients (P5–P7, 17.6 ± 0.9 pF, n = 19; P12–P14, 20.9 ± 1.3 pF, n = 12; p = 0.014 t test).

ΔC_m was measured after single 1 ms depolarizations ($\Delta C_{m(single)}$), pairs of 1 ms depolarizations (10 ms interval, $\Delta C_{m(pair)}$), and 100 Hz trains of 15 1 ms depolarizations ($\Delta C_{m(train)}$; Figures 4B, 4C, and 4E). For depolarizations to 0 mV, $\Delta C_{m(single)}$ ranged from 15 fF to 88 fF in immature and from 57 fF to 135 fF in mature calyces. From P5 to P14, the mean $\Delta C_{m(single)}$ approximately doubled (Figure 4E, Table 2). We observed a positive correlation between resting C_m and $\Delta C_{m(single)}$ (Figure 4D), suggesting that larger calyces released more vesicles. A similar correlation was also observed in pituitary nerve terminals (Hsu and Jackson, 1996) and bipolar cells (von Gersdorff et al., 1996). Values for $\Delta C_{m(single)}$ in terminals with mono- and double-exponentially decaying passive charging transients were not significantly different and were therefore pooled in Table 1 (e.g., at P12–P14, ΔC_m was 84 ± 13 fF [n = 4] and 92.8 ± 13 fF [n = 6] for calyces requiring mono- and double-exponential fits, respectively).

$\Delta C_{m(pair)}$ was on average ~95% (P5–P7) and ~80% (P12–P14) larger than $\Delta C_{m(single)}$, indicating little paired pulse depression of exocytosis (Figure 4E; Sun et al., 2002). Values for $\Delta C_{m(train)}$ were significantly larger than $\Delta C_{m(single)}$ or $\Delta C_{m(pair)}$ and ranged from 135 fF to 437 fF for P5–P7 and from 219 fF to 639 fF for P12–P14 terminals. On average, $\Delta C_{m(train)}$ increased >90% during development (Figure 4E, Table 2). However, $\Delta C_{m(train)}$ was smaller than the projected values in the absence of depression (i.e., 15 × $\Delta C_{m(single)}$) for both age groups. Nevertheless, as for paired pulses, the amount of depression during 100 Hz trains was similar in immature and mature synapses: $\Delta C_{m(train)}$ was about 37% (P5–P7) and about 35% (P12–P14) of the value 15 × $\Delta C_{m(single)}$. This finding contrasts with previous results for 100 Hz EPSC trains, which showed much stronger depression in immature than in mature synapses (Iwasaki and Takahashi, 2001; Taschenberger and von Gersdorff, 2000).

Since we surmised that Q_{Ca} elicited in P12–P14 termi-

Table 2. Passive Properties and C_m Recordings in Immature (P5–P7) and Mature (P12–P14) Calyces

	P5–P7	P12–P14	
Passive Properties			
C_m (pF)	43.9 ± 2.0 (19)	44.8 ± 3.2 (12)	$p > 0.05$
R_s (MΩ)	18.3 ± 1.2 (19)	16.7 ± 1.4 (12)	$p > 0.05$
R_m (GΩ)	1.38 ± 0.18 (19)	1.26 ± 0.35 (12)	$p > 0.05$
τ_{fast} (μs)	186 ± 17 (19)	220 ± 24 (12)	$p > 0.05$
% fast	72 ± 3 (19)	75 ± 5 (12)	$p > 0.05$
τ_{slow} (ms)	1.34 ± 0.25 (19)	1.17 ± 0.19 (12)	$p > 0.05$
Single Depolarization			
1 ms, 0 mV			
Q_{Ca} (pC)	−1.60 ± 0.17 (9)	−1.75 ± 0.19 (10)	$p > 0.05$
ΔC_m (fF)	43.7 ± 6.4 (9)	89.4 ± 8.9 (10)	$p = 0.006$[a]
AP waveform			
Q_{Ca} (pC)	−1.52 ± 0.12 (9)	n.a.	n.a.
1 ms, +40 mV			
Q_{Ca} (pC)	n.a.	−1.44 ± 0.27 (3)	n.a.
ΔC_m (fF)	n.a.	61.0 ± 11.0 (6)	n.a.
Train of Depolarizations			
15 × 1 ms, 0 mV			
Q_{Ca} (pC)	−27.2 ± 3.1 (9)	−32.8 ± 5.6 (7)	$p > 0.05$
ΔC_m (fF)	239 ± 28 (9)	456 ± 60 (7)	$p = 0.008$[a]
15 × 1 ms, +40 mV			
Q_{Ca} (pC)	n.a.	−23.77 ± 5.13 (3)	
ΔC_m (fF)	n.a.	273.8 ± 32.5 (6)	

Membrane capacitance (C_m) and resistance (R_m) were calculated from the current integral and the steady-state current of charging transients elicited by hyperpolarizing pulses from V_h (−80 mV) to −90 mV. The AP waveform used as the voltage command for P5–P7 calyces was obtained from an afferent fiber stimulation-evoked AP recorded in current-clamp in a P6 terminal. In addition to depolarizing pulses to 0 mV, depolarizations to +40 mV were used in some mature calyces to mimic mature AP waveforms (see Results). Statistical comparisons were made using Mann-Whitney U test.

n.a. = not available

[a] $p < 0.01$

nals by depolarizations to 0 mV (1 ms) is larger than AP-evoked Ca influx, we also tested more AP-like depolarizations (+40 mV, 1 ms; Figures 4B and 4C, right). These yielded smaller $\Delta C_{m(single)}$ values (53 fF to 113 fF) that were on average only 30% larger than $\Delta C_{m(single)}$ at P5–P7 (Figure 4E, Table 2). This result parallels the similarity in mean EPSC amplitudes at the two developmental stages (see below). The ratio between $\Delta C_{m(train)}$ and the value $15 \times \Delta C_{m(single)}$ was, however, similar for depolarizations to +40 mV or 0 mV (Table 2). With a mean vesicle diameter of 50 nm (see EM measurements above), and assuming a specific membrane capacitance of 10 fF/μm², we estimate the average number of vesicles released by single AP-like depolarizations to be ~560 for P5–P7 and ~780 for P12–P14.

Developmental Increase in the Efficiency of Exocytosis

We next compared the relationship between Ca influx and ΔC_m during development. As noted above, Q_{Ca} elicited by short depolarizations (0 mV, 1 ms) was on average only 9.3% larger in P12–P14 compared with P5–P7 calyces (Table 2). Even taking into account a fourth power relationship between Q_{Ca} and ΔC_m (Borst and Sakmann, 1996), the relatively small increase from P5 to P14 in Q_{Ca} elicited by 1 ms depolarizations can only partially (i.e., 43%) account for the more than doubling of $\Delta C_{m(single)}$ during development. In fact, when terminals with similar Q_{Ca} were compared, a much larger $\Delta C_{m(single)}$ was observed for P12–P14 (Figure 5A). For 1 ms depolarizations to 0 mV, the average $\Delta C_m/Q_{Ca}$ increased from 28 ± 4 fF/pC (n = 11) to 46 ± 4 fF/pC (n = 6; Figure 5B), which corresponds to an increase from 355 to 585 vesicles/pC from P5 to P14.

The developmental increase in exocytosis efficiency also holds true for longer pulse durations. For prolonged depolarizations (>5 ms), the difference between Q_{Ca} in immature and mature calyces was generally larger (Figure 5C), presumably because I_{Ca} did not fully activate during 1 ms step depolarizations. For example, 50 ms depolarizations elicited mean peak I_{Ca} amplitudes of 1.0 ± 0.1 nA (P6–P7, n = 6) and 1.6 ± 0.2 nA (P11–P12, n = 5). This developmental increase in I_{Ca} is consistent with previous reports (Chuhma and Ohmori, 1998), and it could compensate for the shorter AP widths, which would per se reduce Ca influx and release (Borst and Sakmann, 1999; Lin and Faber, 2002). However, for any given value of Q_{Ca}, the corresponding ΔC_m was at least one-third higher in mature terminals (Figure 5D). ΔC_m started to plateau for depolarizations longer than 30 ms, presumably because of depletion of releasable vesicles. Previous ΔC_m measurements plateaued at 10 to 30 ms (Sun and Wu, 2001), but note that we use 0.2 mM EGTA in our pipette solution, a concentration that does not alter the EPSC amplitude (Borst and Sakmann, 1996) but is 4-fold higher than the 0.05 mM BAPTA used by Sun and Wu (2001). The mean ΔC_m elicited by the strongest stimuli used in this study (100 ms, 0 mV) amounted to

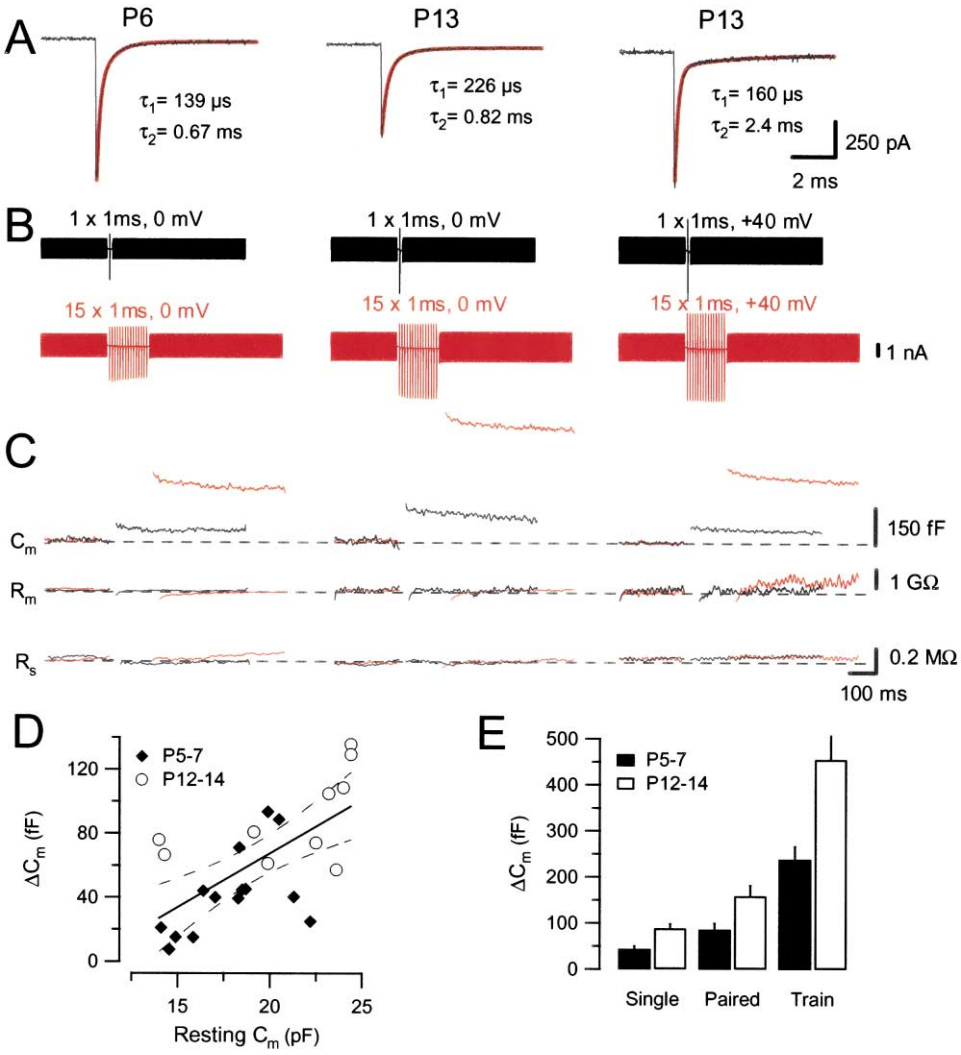

Figure 4. Exocytosis Measured by Membrane Capacitance Recordings Elicited by Single and Repetitive AP-like Depolarizations

(A) Passive membrane properties of one P6 and two P13 terminals are compared by analyzing transient capacitive currents evoked during a brief hyperpolarization from $V_h = -80$ mV to -90 mV. The decay of the transient currents was fitted with a double-exponential function (red superimposed curve). Values for τ_{fast} and τ_{slow} (labeled as τ_1 and τ_2, respectively) are given next to each trace.

(B) Voltage protocol for ΔC_m measurements from the same calyces shown in (A). A 1 kHz sine wave voltage command was applied before and after a single (black trace) or a train of 15 depolarizing steps of 1 ms duration (100 Hz, red trace). Terminals were depolarized to 0 mV (left and middle) or to +40 mV (right).

(C) Corresponding changes in C_m. ΔC_m (top trace) did not correlate with changes in R_m (middle trace) or R_s (bottom trace). The resting C_m was similar for the three terminals: 18.7 pF (P6), 20.2 pF (P13, middle column), and 19.4 pF (P13, right column).

(D) Scatter plot of resting C_m versus ΔC_m (elicited by 1 ms step depolarizations to 0 mV) for a total of 24 terminals (black diamonds: P5–P7, n = 14; open circles: P12–P14, n = 10). A positive correlation between resting C_m values and ΔC_m was observed (solid and dotted lines indicate linear regression and 95% confidence limits, respectively).

(E) Mean values for ΔC_m measured after single pulses, double pulses (10 ms interpulse interval), and trains of 15 pulse depolarizations at 100 Hz for P5–P7 (black bars) and P12–P14 terminals (white bars). All pulses were 1 ms depolarizations to 0 mV from a $V_h = -80$ mV. Mature terminals had a greater exocytotic capacity.

368 ± 52 fF (P5–P7) and 660 ± 77 fF (P11–P14), indicating that the number of vesicles available for release during prolonged depolarizations is significantly larger in mature terminals (~4685 versus ~8405 vesicles).

Reduction of Synaptic Depression by Kynurenate in Immature Synapses

The observed discrepancy in immature synapses between the amount of depression seen in ΔC_m measurements and in EPSC recordings could indicate that postsynaptic mechanisms contribute to synaptic depression (Scheuss et al., 2002). In order to prevent AMPA-R desensitization due to rebinding of residual glutamate, we recorded EPSCs in the presence of a high concentration (1 mM) of the low-affinity antagonist kynurenic acid (KYN). Although the rates for KYN binding and unbinding at synaptic AMPA-R expressed in the MNTB are unknown, one can estimate that >95% of the receptors

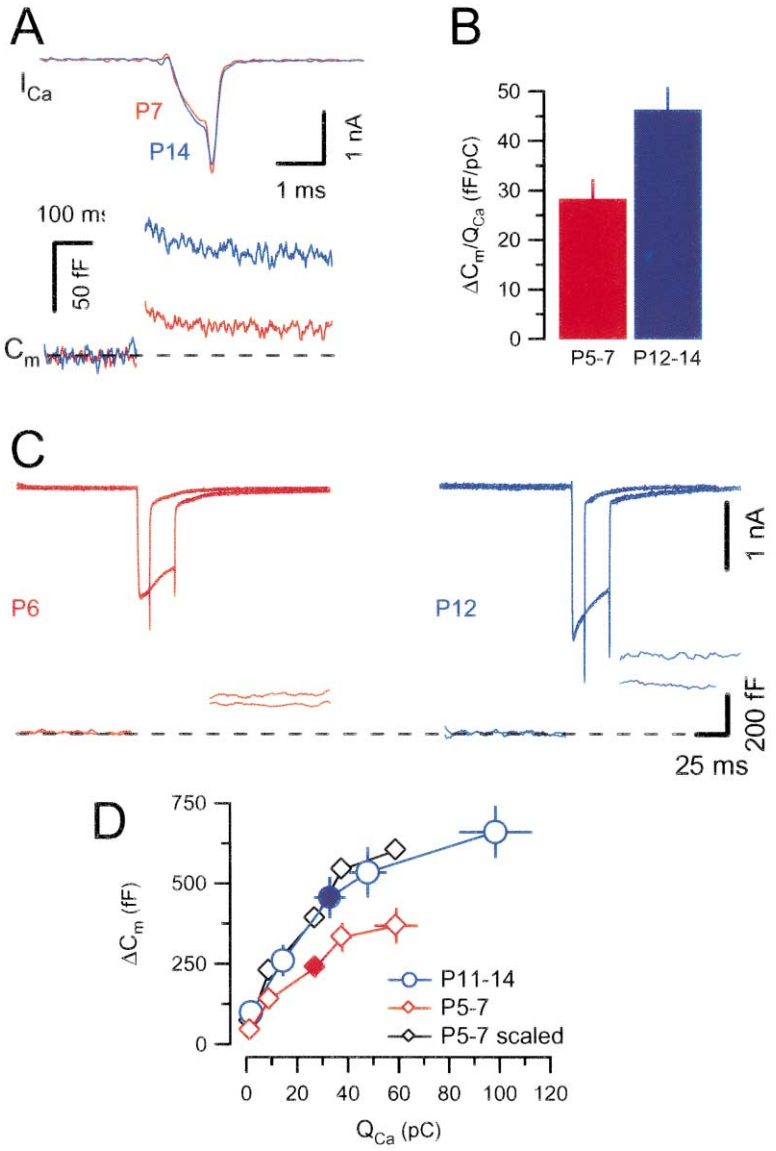

Figure 5. Higher Efficiency of Exocytosis in Mature Terminals

(A) Recordings of I_{Ca} and ΔC_m from P7 and P14 calyces voltage-clamped at $V_h = -80$ mV and depolarized to 0 mV for 1 ms. Resting C_m: 22.2 pF (P7), 14.4 pF (P14). Although I_{Ca} was similar in both terminals, ΔC_m was considerably larger in the mature terminal.

(B) Mean values for $\Delta C_m/Q_{Ca}$ for 1 ms step depolarizations (0 mV). $\Delta C_m/Q_{Ca}$ was on average about 64% larger in P12–P14 terminals.

(C) Changes in C_m in response to prolonged depolarizations (10 and 30 ms, 0 mV) in a P6 and a P12 terminal. Resting C_m: 13.4 pF (P6), 18.8 pF (P12).

(D) Scatter plot of ΔC_m versus Q_{Ca} for depolarizing pulses (0 mV) of various durations (1 to 100 ms, $n \geq 7$ cells for each data point). For any given amount of Ca influx, a larger corresponding ΔC_m was measured in mature terminals. Moreover, comparison of the scaled curve (164%, black line) of the P5–P7 data with the data for P12–P14 suggests similar Ca sensitivity and time course of release at both ages. Filled symbols denote results obtained from experiments using trains as shown in Figure 4.

are occupied by KYN at a concentration of 1 mM based on previous modeling work and recordings from cultured hippocampal neurons (Diamond and Jahr, 1997). Following presynaptic APs, the peak glutamate concentration in the synaptic cleft is high enough to cause a large fraction of KYN to be displaced by glutamate and thereby generate an EPSC. We reasoned that, in the presence of KYN, the fraction of AMPA-R entering a desensitized state might be greatly reduced because KYN prevents binding to glutamate of a large fraction of the AMPA-R. In addition, after opening, most receptors will rebind KYN due to its faster binding rate and much higher concentration than residual glutamate. KYN bound receptors will then be available for opening during the subsequent release event.

Figure 6A illustrates 100 Hz trains of EPSCs recorded in the absence and presence of 1 mM KYN. The first EPSC in the trains was inhibited slightly less by KYN in P5–P7 synapses (26% ± 1% of control, n = 11) compared with P12–P14 (20% ± 2% of control, n = 10). For comparison, control EPSC trains and those recorded in the presence of KYN are superimposed after normalizing to the peak of the first control EPSC (Figure 6A, right). The amount of inhibition by KYN in immature synapses was greatly reduced later in a train, especially for the second and third EPSCs. On average, the second EPSC and the last EPSC in the train were 61% ± 5% and 40% ± 3% of control. In P5–P7 synapses, the reduced KYN inhibition during trains resulted in less synaptic depression compared with control conditions (Figures 6B and 6C). In contrast to P5–P7 synapses, at P12–P14 the average amount of inhibition by KYN was nearly uniform among all EPSCs in the train, and depression was unchanged by KYN (23% ± 2% of control for the second EPSC and 18% ± 2% of control for the last EPSC; Figures 6).

Reduced AMPA Receptor Desensitization in Mature Synapses

The results described above suggest that AMPA-R desensitization affects EPSC trains in immature but not mature synapses. We thus predict that cyclothiazide

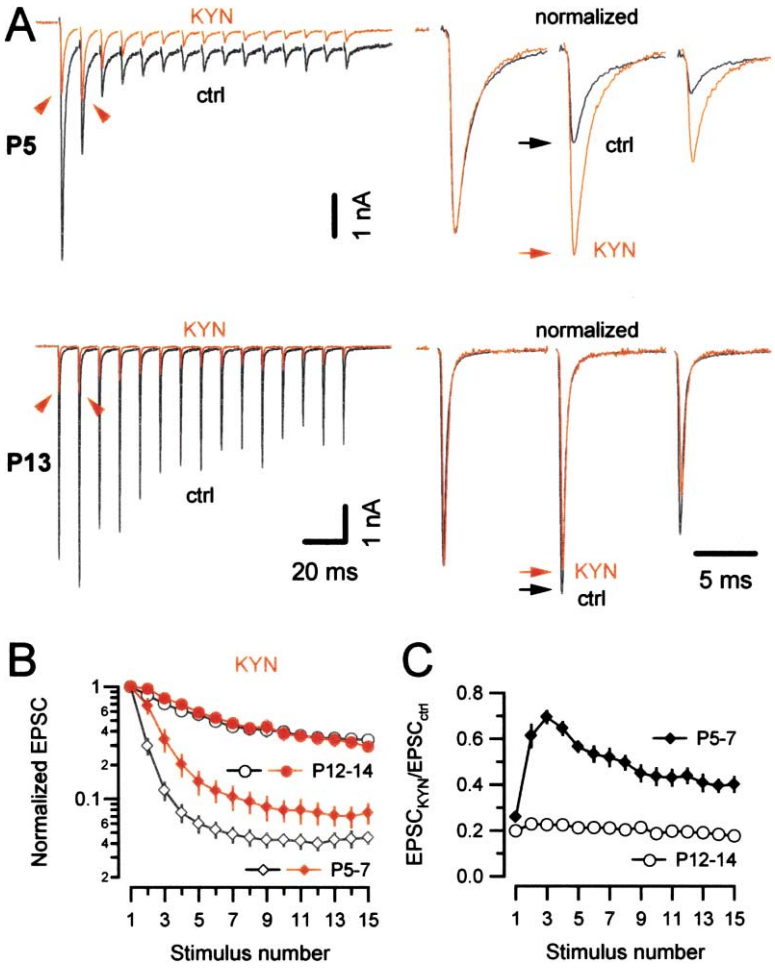

Figure 6. KYN Reduced Synaptic Depression in P5–P7 but not P12–P14 Synapses

(A) Left, trains of 15 EPSCs evoked by high-frequency stimulation (100 Hz) in a P5 (top trace) and a P13 MNTB cell (bottom trace) recorded in the absence (black) and presence (red) of KYN. First, three EPSCs are shown superimposed at a higher time resolution (right) after normalizing to the peak of the initial EPSC in the control train. In the P5 synapse, KYN inhibited the later responses much less than the initial EPSC, whereas at P13 all EPSCs in the train were reduced similarly. NMDA receptors blocked by 50 μM D-APV.

(B) Synaptic depression is reduced in the presence of KYN (red symbols) in P5–P7 (n = 11) but not in mature synapses (n = 10). Vertical lines on symbols indicate SEM.

(C) $EPSC_{kyn}/EPSC_{ctrl}$ calculated for each EPSC during the train and plotted versus stimulus number. Note the reduced inhibition of the steady-state EPSC (last five EPSCs) at P5–P7.

(CTZ), a drug that slows AMPA-R desensitization, would have little effect at P12–P14 (Wang and Kaczmarek, 1998). However, the interpretation of such experiments is complicated by the fact that the efficacy of CTZ depends strongly on the particular AMPA-R subunit composition. For example, CTZ blocks desensitization of recombinant AMPA-R very effectively for homomeric flip splice variants, or heteromeric AMPA-R that contain at least one flip subunit, whereas it is much less effective for flop homomers (Partin et al., 1994). On the other hand, PEPA (Sekiguchi et al., 1997) and aniracetam (ANI; Brenowitz and Trussell, 2001) are more effective for flop splice variants.

The expression of AMPA-R subunits in MNTB is developmentally regulated (Caicedo and Eybalin, 1999; Parks, 2000). It is thus possible that synaptic AMPA-R change during development from little flop to predominantly flop subunit-containing receptors, given the prominent acceleration in mEPSCs kinetics with age (Taschenberger and von Gersdorff, 2000). We therefore tested both the flip splice variant-preferring compound CTZ and the flop splice variant-preferring compounds PEPA (200 μM) and ANI (4 mM) for their effects on synaptic depression (Figure 7). CTZ was used at a relatively low concentration (50 μM) to reduce its effects on release probability (Ishikawa and Takahashi, 2001).

CTZ, PEPA, and ANI increased peak amplitudes and slowed the decay of EPSCs (Figure 7A). The latter effect was most obvious for CTZ in P5–P7 synapses and less pronounced in mature synapses (Joshi and Wang, 2002). CTZ also significantly reduced depression in P5–P7 synapses, whereas no effect was seen in mature synapses (Figure 7B). In contrast, neither PEPA nor ANI affected synaptic depression in immature or mature synapses (Figures 7C and 7D). The strong reduction by CTZ of depression in immature synapses suggests that their AMPA-R probably contain flip splice variants, whereas the lack of effect of CTZ and PEPA in mature synapses does not allow us to draw conclusions about AMPA-R subunit composition. Taken together, these results strengthen the notion that desensitization of AMPA-R does not contribute significantly to synaptic depression at 100 Hz in mature synapses.

Multivesicular Release at Immature AZs

Under conditions that prevent AMPA-R saturation and largely antagonize receptor desensitization, the cumulative EPSC ($EPSC_{cum}$) may be used to compare the total number of released quanta during trains in immature and mature synapses. We compared $EPSC_{cum}$ under control conditions (Figure 8A) and in the combined presence of 1 mM KYN and 50 μM CTZ (Figure 8B). The control $EPSC_{cum}$ in P5–P7 synapses was 28% of the value obtained for P12–P14 synapses (19.2 ± 3.2 nA versus

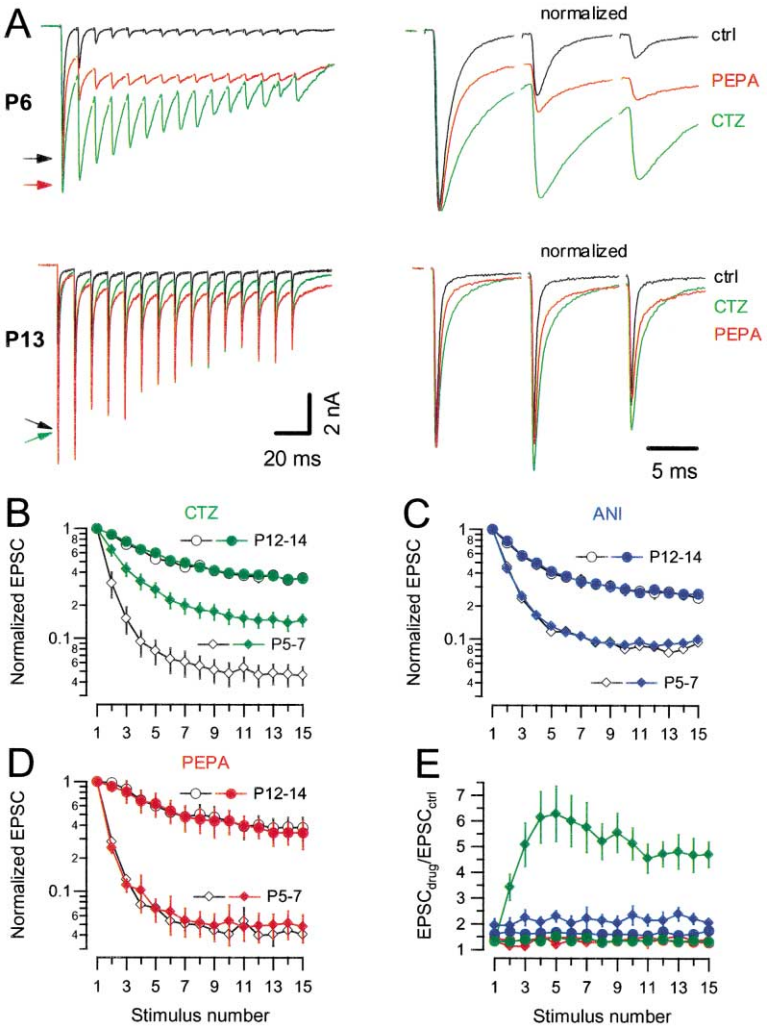

Figure 7. Reduced AMPA-R Desensitization during Repetitive Stimulation in P12–P14 Synapses

(A) 100 Hz trains of 15 EPSCs in a P6 (top) and a P13 MNTB cell (bottom) in control solution and in the presence of CTZ (50 μM) or PEPA (200 μM). First three EPSCs are shown superimposed at a higher time resolution (right) after normalizing to the peak of the initial EPSC in the control train. NMDA receptors were blocked by 50 μM D-APV.

(B–D) CTZ (50 μM, B), but not ANI (4 mM, C) and PEPA (200 μM, D), reduces synaptic depression in P5–P7 but not P12–P14 animals. Comparisons between control and drug (open and filled symbols, respectively) were made after normalizing each EPSC to the first response in the train (n = 4–9).

(E) Relative enhancement of EPSCs in the presence of CTZ (green), ANI (blue), and PEPA (red). The ratio of $EPSC_{drug}/EPSC_{ctrl}$ was calculated for each EPSC during the train and plotted versus stimulus number for the experiments summarized in (B)–(D). Vertical lines on symbols indicate SEM.

69.6 ± 6.2 nA). With quantal amplitudes of 28.7 ± 3.0 (n = 5 cells, 5095 mEPSCs) and 42.8 ± 5.6 pA (n = 8 cells; 4911 mEPSCs), for P5–P7 and P12–P14, respectively, the $EPSC_{cum}$ thus corresponds to approximately 670 quanta (P5–P7) versus 1630 quanta (P12–P14). However, with KYN + CTZ present in the bath, the $EPSC_{cum}$ measured for P5–P7 grew to 65% of the value for P12–P14 (23.9 ± 4.0 nA versus 36.7 ± 4.8 nA). Thus, the number of released quanta is vastly underestimated for immature synapses under control conditions (Scheuss et al., 2002). Since individual mEPSCs in the presence of KYN + CTZ were too small to be reliably detected, we estimated their amplitude by assuming that mEPSCs are similarly reduced by KYN + CTZ as are evoked EPSCs (48.6% ± 4.2% for P5–P7 and 47.5% ± 3.9% for P12–P14). Based on such assumptions (quantal amplitude 13.9 versus 20.3 pA), at least 1717 ± 289 (P5–P7) and 1809 ± 237 (P12–P14) quanta were released during 100 Hz trains of 15 stimuli.

In order to compare the amount of depression in presynaptic C_m and postsynaptic EPSC recordings, we calculated the ratio between the first and the cumulative responses for EPSCs ($EPSC_1/EPSC_{cum}$) as well as for ΔC_m ($\Delta C_{m1}/\Delta C_{m15}$). Under control conditions, $EPSC_1/EPSC_{cum}$ was 51.9% ± 5.6% in P5–P7 but only 13.1% ± 0.7% in P12–P14 MNTB cells. In the presence of CTZ + KYN, however, this value was reduced to 22.7% ± 3.7% for P5–P7 terminals but virtually unchanged for mature synapses (13.0% ± 0.9%; Figure 8C). For P5–P7 calyces, estimates similar to the values for EPSCs in KYN + CTZ were obtained for capacitance measurements ($\Delta C_{m1}/\Delta C_{m15}$ = 22.7% ± 3.8%). For P12–P14 terminals, $\Delta C_{m1}/\Delta C_{m15}$ was slightly higher than $EPSC_1/EPSC_{cum}$ (22.4% ± 2.5%).

We next estimated the probability of release for a single quantum (P_{ves}) using the method of Elmquist and Quastel (1965). This approach is based on a simple depletion model of depression, which assumes that EPSC amplitudes decrease proportionally to the number of remaining quanta during repetitive stimulation (Lu and Trussell, 2000). When EPSC amplitudes are plotted versus cumulative release, an extrapolation of a regression line to the first EPSC amplitudes in a train provides an estimate for the total amount of releasable quanta, which was proportional to 19.3 nA (P5–P7, 1390 quanta) and 36.4 nA (P12–P14, 1790 quanta; arrows in Figure 8D). P_{ves} can be calculated as the ratio between the first EPSC and the total pool size, yielding values of 0.28

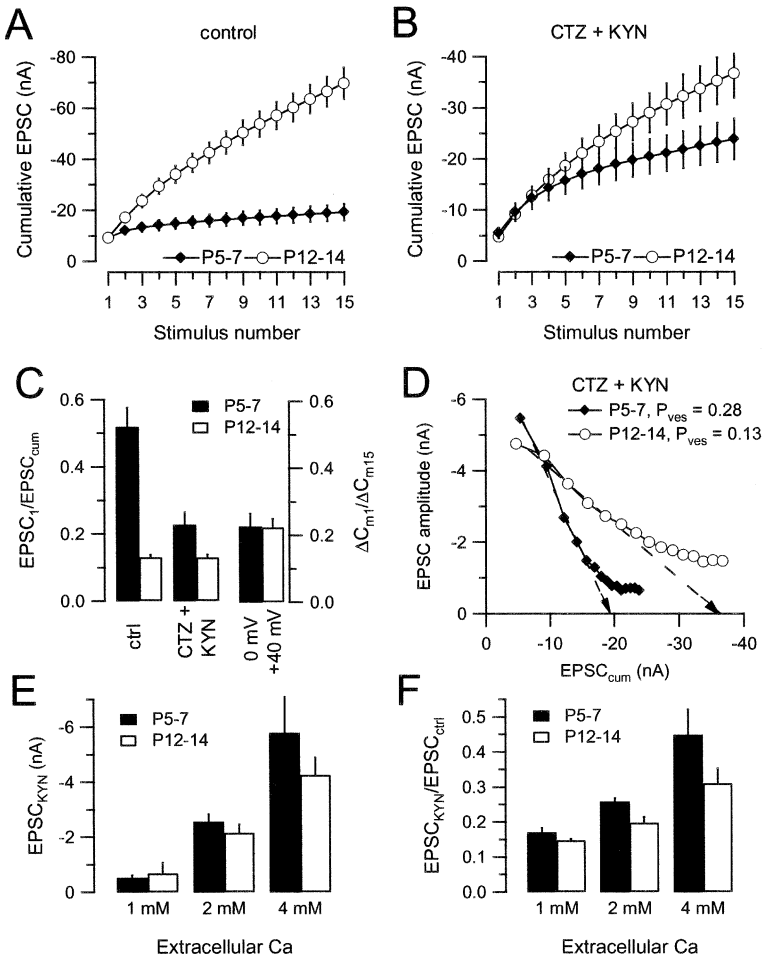

Figure 8. Estimation of Vesicle Pool Size and Initial Release Probability (P_{ves})

(A and B) Cumulative amplitudes of 100 Hz EPSC trains in P5–P7 (black diamonds) and P12–P14 (open circles) MNTB principal cells recorded in control solution (A) and in the combined presence of CTZ (50 μM) + KYN (1 mM) (B). The difference in cumulative EPSCs between P5–P7 and P12–P14 is greatly reduced under conditions when AMPA-R saturation and desensitization are blocked. In the absence of KYN and CTZ, cumulative EPSCs thus underestimated the total amount of release in immature synapses.

(C) Plot of first amplitudes over summed response for 100 Hz trains of EPSCs (cumulative EPSC, left two pairs of bar graphs) or ΔC_m measurements (ΔC_{m15}, right pair of bar graphs). Under control conditions, $EPSC_1$ contributed >50% to the cumulative EPSC at P5 but <15% at P12–P14. In the presence of CTZ + KYN, this value was reduced to about 20% for immature synapses but virtually unchanged at P12–P14. Values for $\Delta C_{m1}/\Delta C_{m15}$ were similar to the ratio of EPSCs in CTZ + KYN. Note that P5–P7 terminals were depolarized to 0 mV, while P12–P14 terminals were depolarized to +40 mV in these experiments in order to account for a reduction in I_{Ca} due to the briefer presynaptic APs of P12–P14 calyces.

(D) Plot of EPSCs versus cumulative EPSC to estimate probability of release of a single quantum (P_{ves}). Line fit to first five data points; arrows show the initial vesicle pool size. Mean values for P_{ves} were 0.28 (P5–P7) and 0.13 (P12–P14).

(E) Mean EPSC amplitudes increased with increasing Ca concentration in the presence of 1 mM KYN. Elevating normal external Ca (2 mM) to 4 mM augmented EPSC amplitudes on average by ~125% and ~100% for P5–P7 and P12–P14, respectively.

(F) Amount of KYN inhibition decreased with increasing external Ca concentration. When release probability was low (1 mM Ca), EPSCs were antagonized to a similar degree by KYN for both age groups. The amount of inhibition was more sensitive to changes in external Ca at P5–P7 compared to mature synapses.

(P5–P7) and 0.13 (P12–P14; Figure 8D). For P12–P14, P_{ves} estimated from control EPSC trains was similar (P_{ves} = 0.15) to the value obtained in the presence of CTZ + KYN, which is consistent with a very minor contribution of postsynaptic effects to depression in P12–P14, and also suggests that CTZ did not significantly affect P_{ves} (Ishikawa and Takahashi, 2001). Notice that after the first five stimuli, the data points in Figure 8D eventually deviate from a straight line, suggesting that a replenishment process may augment the number of released quanta late in the stimulus train (Wang and Kaczmarek, 1998). In addition, this deviation may indicate changes in P_{ves} during the train (Wu and Borst, 1999), suggesting that a simple depletion model is probably not valid throughout the whole train.

Our estimates for P_{ves} are much lower than those of Iwasaki and Takahashi (2001) (0.75 for P7 and 0.29 for P14, but see Meyer et al., 2001). If P_{ves} is indeed low for both immature and mature synapses, one would predict a large increase in EPSCs when P_{ves} is experimentally elevated, for example by raising external Ca (Schneggenburger et al., 1999). Figure 8E summarizes experiments in which external Ca was varied over a large range (1 to 4 mM). In order to prevent AMPA-R saturation, 1 mM KYN was added to the bath. Under these conditions, a large increase in EPSC size with increasing Ca concentration was observed for both immature and mature synapses, lending support to our estimate of low P_{ves} for both ages. Since the amount of EPSC inhibition by KYN is sensitive to changes in peak concentration of the glutamate transient in the synaptic cleft, we plotted $EPSC_{KYN}/EPSC_{ctrl}$ for different external Ca concentrations. The ratio $EPSC_{KYN}/EPSC_{ctrl}$ did not depend on the $EPSC_{ctrl}$ amplitude, which varied from 5 to 22 nA, suggesting adequate voltage clamp (data not shown). Increasing external Ca reduced the amount of KYN inhibition (Figure 8F). The latter effect is more pronounced for immature synapses, which is consistent with the assumption of a higher peak glutamate concentration in the synaptic cleft of immature synapses. This could render AMPA-R in P5–P7 more susceptible to saturation than those in mature synapses. Such differences in glutamate concentration could arise from pooling of transmitter between neighboring release sites (Trussell et al., 1993;

DiGregorio et al., 2002) or the release of multiple quanta per AZ (Auger et al., 1998; Wadiche and Jahr, 2001).

Discussion

Several pronounced ultrastructural and functional changes occur at the calyx of Held synapse from P5 to P14, a period when this synapse extends its range for high-frequency transmission from less than 300 Hz to more than 800 Hz (Borst et al., 1995; Taschenberger and von Gersdorff, 2000). We propose that these changes optimize the mature synapse for prolonged, high-fidelity transmission at near-kHz frequencies.

Synaptic Ultrastructural Changes during Development

Maturation of the cup-shaped calyx to the adult branched form occurs between P5 and P14 in rats (Kandler and Friauf, 1993), proceeding along a developmental sequence originally described by Morest (opossum: 1967). At these ages, the fraction of MNTB cell body surface apposed to the calyx (about 60%) is somewhat higher than that reported for adult cats (40%–50% in Smith et al., 1998), perhaps reflecting a developmental stage prior to additional pruning of the calyx as it completes its maturation. Figure 1 shows that the calyceal stalks are separated from each other at P14, like intracellularly labeled calyces in adult rodents (Kuwabara et al., 1991). This arrangement of calyx elements along the cell surface in single-electron micrographs resembles ultrastructural observations of HRP-labeled calyces in adult cats (Smith et al., 1991). Here we have demonstrated that the average size of AZs, determined by the dimensions of the PSD, decreases from P5 to P14. The absence of large PSDs in our older animals may be due to a breakup of large PSDs at P5 into smaller components by P14. A similar transition in PSD size with age occurs in the hippocampus (Harris et al., 1992). The PSD is a dynamic structure, whose thickness can increase with activity levels over a period of minutes due to protein binding (Dosemeci et al., 2001). Likewise, the surface area of AZs and PSDs may also reflect neural activity. In the end bulbs of Held, PSDs are smaller, and more numerous, in synapses originating from fibers with high levels of spontaneous activity in vivo (Ryugo et al., 1996). In congenitally deaf cats, an increase in AZ size was noticed by six months of age in these synapses, which may compensate for decreased electrical activity (Redd et al., 2000), and P_r is higher in congenitally deaf mice ($P_r = 0.8$) than in hearing animals ($P_r = 0.5$; Oleskevich and Walmsley, 2002). Similarly, AZ and PSD area increase in parallel, and proportionally to P_r, after activity is silenced by TTX in neuronal cultures (Murthy et al., 2001). We propose that the decreasing size of AZs in the calyx of Held supports an age-related increase in levels of neuronal activity. Small AZs may also be better suited to support rapid local endocytosis since they allow more space for the endocytotic machinery in the periphery of AZs (Roos and Kelly, 1999; Teng and Wilkinson, 2000).

The size of PSDs that we report is similar in range to those in other studies of large terminals in the auditory system (Ryugo et al., 1996; Rowland et al., 2000; Nicol and Walmsley, 2002). In the calyx, the fraction of surface area devoted to AZs is similar at P5 and P14 and consistent with the analysis of one completely reconstructed calyx from a P9 rat that also revealed about 5% of the apposition area to be occupied by AZs (Sätzler et al., 2002). That calyx contained about 600 AZs with a mean surface area 0.089 μm^2, each averaging $\sim$2 docked vesicles. Those numbers fall within the range of values bracketed by our analysis of four P5 and four P14 calyces, all located in the medial (high frequency) one-third of the MNTB, except that the average number of docked vesicles per AZ was greater (about 6.0 at P5 and 3.0 at P14) in our material. Common to all these studies is a linear relationship between PSD or AZ size and the number of anatomically docked vesicles (Schikorski and Stevens, 1997; Nicol and Walmsley, 2002). Clustering of synaptic vesicles near the AZ is prominent at P5, suggesting that a large percentage of vesicles already undergo release and recycling at this early age. We also observed that the number of puncta adhaerentia approximately doubled from P5 to P14. This may help to stabilize the synaptic cleft during periods of continuous exocytosis, which could otherwise detach or shift the precise location of the presynaptic membrane (Rowland et al., 2000).

Vesicle Pool Size Increases during Development

We estimated from our EM data that the total number of docked vesicles per calyx increases by 25% (from 1700 at P5 to 2120 at P14). Recent EM studies in cultured neurons using single sections also report that the number of docked vesicles increases with days in vitro (Renger et al., 2001; Mozhayeva et al., 2002). From EPSC measurements in CTZ + KYN, we estimated a similar (29%) increase in the number of releasable quanta (i.e., the pool size increases from 1390 at P5–P7 to 1790 at P12–P14). Given the uncertainties involved, the agreement between the two estimates seems reasonable. Fluctuation and covariance analysis have been used to estimate a releasable pool size of about 2000 vesicles in P8–P10 calyces (Schneggenburger and Neher, 2000; Sakaba and Neher, 2001; Scheuss et al., 2002). Using KYN + CTZ, we also calculated that 1717 $\pm$ 289 (P5–P7) and 1809 $\pm$ 237 (P12–P14) quanta were released during 100 Hz trains of 15 stimuli. Thus, a similar number of quanta are released at both ages by such stimuli, as suggested also by ΔC_m for train depolarizations (Table 2). Our C_m measurements suggest that a single AP-like stimulus releases 560 (P5–P7) to 720 (P12–P14) vesicles. The P5–P7 value is similar to a report for P8–P10 terminals (450; Sun et al., 2002) but is higher than the quantal content of EPSCs in KYN + CTZ (393 $\pm$ 78 at P5–P7; 234 $\pm$ 37 at P12–P14) or previous estimates from EPSCs recorded under control conditions (210 at P8–P10; Borst and Sakmann, 1996). This discrepancy between C_m and EPSC measurements may be due to asynchronous release that escapes detection in EPSC recordings, or a bias toward larger terminals and effects of whole-cell dialysis in C_m measurements. However, we did find a good agreement in the amount of depression between presynaptic ΔC_m measurements ($\Delta C_{m1}/\Delta C_{m15}$) and EPSC recordings in the presence of KYN + CTZ ($EPSC_1/EPSC_{cum}$) (Figure 8C).

Increases in vesicle pool size may allow mature synapses to transmit high frequencies for more prolonged periods. Indeed, although after 15 AP stimuli the $EPSC_{cum}$ for P5–P7 is only 35% smaller compared with P12–P14 (Figure 8B), the final slope of the curve is very different. Thus, after 50 APs at 100 Hz in KYN + CTZ, the cumulative EPSC reaches values of 46.9 ± 28 nA at P5–P7 and a 88% higher value of 88.2 ± 20 nA at P12–P14. Likewise, C_m measurements using 100 ms step depolarizations (Figure 5C) revealed an 80% larger amount of exocytosis at P12–P14 (~8405 vesicles) compared to P5–P7 (~4685 vesicles). These large numbers clearly suggest that undocked vesicles can be rapidly released during a prolonged presynaptic depolarization. Moreover, note that the scaled P5–P7 curve (black line, Figure 5D) coincides with the P12–P14 data, suggesting that the Ca dependence of exocytosis was similar for both age groups.

Exocytotic Efficiency Increases during Maturation

We found that P12–P14 calyces have larger ΔC_m jumps than P5–P7 for any given amount of Ca influx, suggesting that excitation-secretion coupling is more efficient in mature synapses. At P8–P10, rat calyces of Held express a mixture of R, N, and P/Q type Ca channels (Wu et al., 1999). However, Ca influx via N and R type Ca channels triggers release less effectively than that via P/Q type channels because the former tend to be located further from release sites. Ca channel expression is developmentally regulated with P13 rat calyces expressing predominantly P/Q type (Iwasaki and Takahashi, 1998). In addition, our EM data suggest that the total number of docked vesicles is higher at P12–P14. These changes could explain the higher efficiency of exocytosis in mature terminals. The lower amount of Ca influx needed for exocytosis also reduces the demands for Ca buffering and extrusion during high-frequency stimulation. A close association of P/Q type channel clusters with docked vesicles within smaller AZs could thus be a developmental specialization that makes synaptic transmission faster and more reliable in mature synapses (Mintz et al., 1995; Meinrenken et al., 2002). Changes in presynaptic Ca buffering capacity may also contribute to improvement in synaptic efficiency (Chuhma et al., 2001), and several Ca binding proteins increase in expression levels after P8 in the rat MNTB (Lohmann and Friauf, 1996).

For 1 ms depolarizations to 0 mV, the average $\Delta C_m/Q_{Ca}$ increased from 28 to 46 fF/pC during development (Figure 5B). This equates to about 9000 Ca ions flowing for each released vesicle in P5–P7 synapses, which is about 30% less than the value obtained previously from paired I_{Ca} and EPSC recordings (Borst and Sakmann, 1996). In mature terminals, the number of required Ca ions for each released vesicle is reduced to about 5000. The efficiency of Ca-triggered exocytosis assayed by C_m measurements also increases with age in mouse inner hair cells (Beutner and Moser, 2001). The change in Ca channel density and synaptic efficacy was attributed to ongoing synaptogenesis in hair cells, which alters the morphology of the ribbon-type active zones. However, in contrast to the calyx of Held, long depolarizations (>5 pC of Ca influx) triggered the same amount of exocytosis in P6 and P14–P25 mouse inner hair cells.

Depression Is Predominantly Presynaptic in Mature Synapses

Capacitance measurements using short trains of AP-like stimuli indicated that synaptic depression at 100 Hz has a large presynaptic component in the calyx of Held. The amount of synaptic depression determined from C_m jumps was surprisingly similar in immature and mature synapses. This finding is in sharp contrast with the greatly reduced depression of EPSC trains in mature synapses. We solved this discrepancy by showing that AMPA-R desensitization contributes to depression in immature but not mature synapses (Brenowitz and Trussell, 2001; Joshi and Wang, 2002). For mature synapses, we propose that a predominantly presynaptic mechanism, such as vesicle pool depletion, accounts for depression. We emphasize, however, that AMPA-R in mature synapses may experience a significant amount of desensitization at stimulation frequencies higher than 100 Hz.

Release Probability and Multivesicular Release at Immature AZs

Serial EM reconstructions of bouton-type synapses indicate that they have about eight docked vesicles (Schikorski and Stevens, 1997; Xu-Friedman et al., 2001). By contrast, P14 calyx release sites have about 2–3 docked vesicles, with many sites having no docked vesicles. From a purely morphological standpoint, multivesicular release is thus more likely to occur in P5 than in P14 synapses. Using our estimates for P_{ves} and assuming all docked vesicles are equally fusion competent, we calculate the release of an average of ~1.6 (0.28×5.7, P5–P7) and ~0.4 (0.13×3.3, P12–P14) vesicles per AP from each AZ. Using a binomial model, one would predict that 62% of the successful release events are multivesicular at P5–P7, but only 14% at P12–P14 (Oertner et al., 2002). The glutamate transient following exocytosis may therefore reach higher levels in the cleft of P5 synapses, perhaps leading to a greater number of saturated AMPA-R at that age. Similarly, the average probability for releasing at least one vesicle at an AZ is given by

$$P_r = 1 - (1 - P_{ves})^n,$$

where n = number of fusion-competent vesicles (Hanse and Gustafsson, 2002), and equates to 0.85 (P5–P7) and 0.37 (P12–P14). Interestingly, mean P_r in the climbing-fiber-Purkinje cell synapse is very high (0.9; Silver et al., 1998) and there is evidence for multivesicular release (Wadiche and Jahr, 2001).

Our estimate for P_r at P12–P14 is in reasonable agreement with that calculated for P8–P10 calyces using a variance-mean analysis (0.25–0.4 at individual AZs; Meyer et al., 2001) but lower than those of Chuhma and Ohmori (1998) (0.87 at P9–P11). Our finding that P_r decreases with synapse maturation agrees with recent studies in the MNTB (Iwasaki and Takahashi, 2001), the chick calyx synapse (Brenowitz and Trussell, 2001), and in cultured hippocampal synapses (Chavis and Westbrook, 2001). We emphasize that our estimates for P_r are average values. More detailed analysis shows that release probability may be heterogeneous (Rosenmund et al., 1993; Sakaba and Neher, 2001). The heterogeneity in AZ size we observed may provide an anatomical basis

for P_r heterogeneity (Harris and Sultan, 1995; Meinrenken et al., 2002). Our observation that P_r and the number of docked vesicles per AZ is reduced with age parallels the recent findings of Murthy et al. (2001), who report for cultured hippocampal neurons that the number of docked vesicles correlates positively with P_r. However, the number of vesicles released per AZ is probably not solely dictated by the number of docked vesicles, since synapses with low and high P_r can have the same number of docked vesicles (Xu-Friedman et al., 2001). Indeed, the particular isoforms of proteins involved in the fusion machinery, of Ca binding proteins that regulate Ca buffering, and the exact location of Ca channels are all factors that influence the value of P_r at a given AZ.

Synaptic Architecture May Sculpt the Glutamate Transient

The remodeling of synaptic cleft geometry could have a large impact on the temporal profile of glutamate transients. Following the release of multiple vesicles in an immature calyx, neurotransmitter will be entrapped in the extensive and continuous synaptic cleft (Figures 1 and 2C). Simulations of small bouton-type synapses indicate that after exocytosis the glutamate concentration decays quickly (within $<$1 ms) from peak values $\geq$1 mM (Clements, 1996). However, in calyx-type synaptic clefts, the time course is probably more biphasic and contains a slower decay component that may last tens of milliseconds (Rossi et al., 1995; Otis et al., 1996). Residual glutamate may thus rebind multiple times within the cleft of the cup-shaped immature synapse, causing the desensitization of AMPA-R. In contrast, transmitter released from mature terminals is closer to diffusional exits due to the branched and fenestrated structure of the calyx. In addition, glial processes surrounding mature synapses may be more extensive, more packed with glutamate transporters, and in closer contact with the synapse, leading to more efficient glutamate uptake mechanisms. Together, these factors could additionally reduce residual glutamate and AMPA-R desensitization in P14 calyces. Morphological and molecular changes thus conspire to optimize this synapse during development for sustained high-frequency transmission.

Experimental Procedures

Electron Microscopy

Two P5 and two P14 Sprague-Dawley rat pups were perfused transcardially with a calcium-free Ringer's solution followed by a mixture of 2% paraformaldehyde and 2.5% glutaraldehyde in 0.12 M phosphate buffer. Each brainstem was cut into 200 μm sections in the coronal plane, postfixed with 1% osmium tetroxide, stained en bloc with 2% uranyl acetate, dehydrated, and flat-embedded in Epon. Tissue containing the medial nucleus of the trapezoid body (MNTB), which is innervated by calyces of Held, was reembedded and trimmed for cutting ultrathin sections (65–70 nm). Sequences of 20–33 serial sections were collected and stained with 0.5% uranyl acetate and 3% lead citrate using an automated grid stainer (Leica, Nusslock, Germany), then were viewed using a Jeol 1010 electron microscope. Two calyces from each animal (four at each age), located in the medial, high-frequency portion of the MNTB, were chosen for analysis through a 20 section subset of serial sections.

Photographic montages of the cell perimeters, including the apposed calyces of Held, were assembled at a total magnification of 25–70 K. AZs had at least one synaptic vesicle within 90 nm (two vesicle diameters) of membrane appositions having postsynaptic thickenings and typically dense projections on the presynaptic membrane. Puncta adhaerentia, by contrast, lacked docked vesicles and vesicle clusters and had symmetrical pre- and postsynaptic densities. Montages were viewed under final magnification of 120–160 K in order to measure postsynaptic density lengths. Curved postsynaptic densities (PSDs) were partitioned into 2–3 linear segments in order to closely approximate their total length. The scale bar on the micrograph was verified using photographs, at the same magnifications used for data collection, of a calibration grid provided by the electron microscope manufacturer. Section thickness at the time of cutting was estimated by using the color of tissue floating in the collection well and was calibrated using the cylindrical diameters method (Fiala and Harris, 2001). The surface area of PSDs was calculated by multiplying the summed length across sections by the section thickness. Synaptic vesicles were classified as docked when their membrane and the presynaptic cell membrane were contiguous (i.e., no space between vesicle and plasma membrane), a stringent criteria that may underestimate the number of docked vesicles (see Figure 3 of Lenzi et al., 2002). The numbers of docked vesicles and PSD size were determined only for complete PSDs contained within the series of tissue sections.

Low-magnification images of complete cells and apposed calyces were digitized using a flatbed scanner. MNTB cell perimeters and the length of membrane apposed to calyces were measured using the segmented line drawing tool in NIH Image. These values, summed over all 20 sections, were used to calculate the fraction of MNTB somatic surface in contact with the calyx. Three of four and two of four cells studied at P14 and P5, respectively, were sectioned through their nucleus; all cells had a conspicuous length of calyx apposed to the cell body. The total surface area of both complete and incomplete PSDs was used to calculate the fraction of calyx surface apposed to MNTB cells that was occupied by synapses. These values were scaled to the total surface area of a standard MNTB cell for each age by modeling its geometry as an ellipsoid. The surface areas of the standard cells were the average of measurements from a population of 10 MNTB cells at each age that were sectioned through their nucleus. Separate photographic fields of synaptic vesicles in the vicinity of the AZ were captured at magnification of 50 K and prints were digitized. The outer diameters of vesicles that appeared circular were measured using the line drawing tool of NIH Image. Unless otherwise stated, errors are SEM.

Slice Preparation

Brainstem slices were obtained from P5–P14 Sprague-Dawley rats. After decapitation, the brainstem was quickly immersed in ice-cold low-calcium artificial cerebral spinal fluid (aCSF) containing (in mM) NaCl (125), KCl (2.5), $MgCl_2$ (3.0), $CaCl_2$ (0.1), glucose (25), $NaHCO_3$ (25), NaH_2PO_4 (1.25), ascorbic acid (0.4), myo-inositol (3), and Na-pyruvate (2); the pH was 7.3 when bubbled with carbogen (95% O_2, 5% CO_2). The brainstem was then glued onto the stage of a vibratome slicer (Leica, Germany), and 180–200 μm thick slices were cut proceeding from caudal to rostral. Slices were transferred to an incubation chamber containing normal aCSF bubbled with carbogen and maintained at 35°C for 30 min, and thereafter at room temperature (RT, 22°C–24°C). The normal aCSF was the same as the low-calcium aCSF except that 1.0 mM $MgCl_2$ and 2.0 mM $CaCl_2$ were used.

Electrophysiology

Whole-cell patch-clamp recordings were performed in normal aCSF at RT. During experiments slices were continuously perfused with normal aCSF solution and visualized by IR-DIC microscopy (Axioskop, Zeiss, Germany). The pipette solution for recording presynaptic Ca currents and membrane capacitance changes was composed of (in mM) Cs-gluconate (130), CsCl (15), TEA-Cl (20), Na_2-phosphocreatine (5), HEPES (10), EGTA (0.2), and ATP-Mg (4); pH adjusted to 7.3 with CsOH. TTX (0.5 μM) and TEA (5 mM) were added to the bath to block voltage-activated sodium and potassium currents. For postsynaptic recordings, patch pipettes were filled with a solution consisting of (in mM) CsCl (150), TEA-Cl (10), Na_2-phosphocreatine (2), HEPES (10), EGTA (5), and ATP-Mg (4); pH adjusted to 7.3 with CsOH. Patch pipettes were pulled from soft thin-walled glass (WPI, Sarasota, FL) using a Narishige puller (PP-

830, Japan). Pipettes were coated with dental wax to reduce noise and pipette capacitance. Patch-pipettes had an open tip resistance of 3.0–5.0 MΩ for pre- and 1.5–2.5 MΩ for postsynaptic recordings. Access resistance (R_s) was ≤20 MΩ for calyx recordings and ranged from 2.0 to 4.5 MΩ for postsynaptic neurons. R_s was compensated ~60% for pre- and >70% for postsynaptic recordings. Presynaptic terminals and principal cells were voltage-clamped at a holding potential (V_h) of −80 mV and −70 mV, respectively. No corrections were made for liquid junction potentials. Presynaptic APs were recorded in the fast current-clamp mode of the EPC-9 after adjusting the fast-capacitance cancellation while in cell-attached mode.

For capacitance recordings, a sinusoidal voltage command (1 kHz and 60–70 mV peak-to-peak amplitude) was applied to the presynaptic terminal in addition to V_h. The resulting membrane currents were processed with a software lock-in amplifier (HEKA, Germany) using the method of Lindau and Neher (Gillis, 1995). The reversal potential of the measured DC current was assumed to be 0 mV (Gillis, 1995). During depolarizations, the membrane capacitance was not measured and ≥20 s were allowed between depolarizing pulses for recovery of exocytosis. In control experiments, ΔC_m was measured in a solution containing 0.1 mM Cd^{2+} to block voltage-dependent Ca channels. For step depolarizations to 0 mV with durations of 2, 10, 50, or 100 ms, the average $\Delta C_m = 5.63 \pm 5.83$ fF ($n = 20$; see also Sun et al., 2002), which was not significantly different from zero. ΔC_m was calculated from the average value of C_m 10–50 ms before and after the depolarizing pulse, so that any tail currents had time to decay back to baseline. The decay of C_m back to the baseline (endocytosis) occurred in seconds, indicating that ΔC_m was not underestimated by rapid endocytosis in our experimental conditions.

In order to evoke postsynaptic currents, a bipolar stimulation electrode was placed on the brainstem midline. Stimulation pulses (≤20 V) were applied through a Master-8 stimulator (AMPI, Jerusalem, Israel) and had a duration of 100 μs. Stimulation pulses were controlled using "Pulse" software (HEKA, Germany) and signals were recorded via a double EPC-9 (HEKA, Germany) patch-clamp amplifier. Sampling intervals and filter settings were 10–25 μs and 5 kHz. Spontaneous mEPSCs were captured using a sliding template algorithm as described by Clements and Bekkers (1997). The average mEPSC 20%–80% risetimes were extremely fast: 152.5 ± 11.5 μs (P5–P7) and 92.4 ± 3.0 μs (P12–P14). Anirecetam and D-2-Amino-5-phosphonovaleric acid (D-APV) were obtained from Tocris Cookson (Bristol, UK). PEPA (4-[2-(Phenylsulphonylamino)ethylthio]-2,6-difluorophenoxyacetamide) was a kind gift of Dr. M. Sekiguchi (NCNP, Tokyo, Japan). All other salts and chemicals were obtained from Sigma (St. Louis, MO). Offline analysis was performed using IgorPro software (Wavemetrics, Lake Oswego, OR). Average data are reported as mean ± SEM values.

Acknowledgments

We thank Craig Jahr for comments on the manuscript and Larry Trussell and George D. Pollack for valuable discussions. Janelle Grimes and Brian Pope provided expert technical assistance with electron microscopy. H.T. was partially funded by a HFSP fellowship. H.v.G. was funded by a NIH/NIDCD grant and a Pew Biomedical Research Scholar grant. G.S. was supported by NIH COBRE Grant P20 RR15574, project #4.

Received: August 20, 2002
Revised: November 25, 2002

References

Auger, C., Kondo, S., and Marty, A. (1998). Multivesicular release at single functional synaptic sites in cerebellar stellate and basket cells. J. Neurosci. *18*, 4532–4547.

Bellingham, M.C., Lim, R., and Walmsley, B. (1998). Developmental changes in EPSC quantal size and quantal content at a central glutamatergic synapse in rat. J. Physiol. *511*, 861–869.

Beutner, D., and Moser, T. (2001). The presynaptic function of mouse cochlear inner hair cells during development of hearing. J. Neurosci. *21*, 4593–4599.

Blue, M.E., and Parnavelas, J.G. (1983). The formation and maturation of synapses in the visual cortex of the rat. II. Quantitative analysis. J. Neurocytol. *12*, 697–712.

Borst, J.G.G., and Sakmann, B. (1996). Calcium influx and transmitter release in a fast CNS synapse. Nature *383*, 431–434.

Borst, J.G.G., and Sakmann, B. (1998a). Calcium current during a single action potential in a large presynaptic terminal of the rat brainstem. J. Physiol. *506*, 143–157.

Borst, J.G.G., and Sakmann, B. (1998b). Facilitation of presynaptic calcium currents in the rat brainstem. J. Physiol. *513*, 149–155.

Borst, J.G.G., and Sakmann, B. (1999). Effect of changes in action potential shape on calcium currents and transmitter release in a calyx-type synapse of the rat auditory brainstem. Philos. Trans. R. Soc. Lond. B Biol. Sci. *354*, 347–355.

Borst, J.G.G., Helmchen, F., and Sakmann, B. (1995). Pre- and postsynaptic whole-cell recordings in the medial nucleus of the trapezoid body of the rat. J. Physiol. *489*, 825–840.

Brenowitz, S., and Trussell, L.O. (2001). Maturation of synaptic transmission at end-bulb synapses of the cochlear nucleus. J. Neurosci. *21*, 9487–9498.

Caicedo, A., and Eybalin, M. (1999). Glutamate receptor phenotypes in the auditory brainstem and mid-brain of the developing rat. Eur. J. Neurosci. *11*, 51–74.

Carr, C.E., Soares, D., Parameshwaran, S., and Perney, T. (2001). Evolution and development of time coding systems. Curr. Opin. Neurobiol. *11*, 727–733.

Chavis, P., and Westbrook, G. (2001). Integrins mediate functional pre- and postsynaptic maturation at a hippocampal synapse. Nature *411*, 317–321.

Chen, C., Blitz, D.M., and Regehr, W.G. (2002). Contributions of receptor desensitization and saturation to plasticity at the retinogeniculate synapse. Neuron *33*, 779–788.

Chuhma, N., and Ohmori, H. (1998). Postnatal development of phase-locked high-fidelity synaptic transmission in the medial nucleus of the trapezoid body of the rat. J. Neurosci. *18*, 512–520.

Chuhma, N., Koyano, K., and Ohmori, H. (2001). Synchronization of neurotransmitter release during postnatal development in a calyceal presynaptic terminal. J. Physiol. *530*, 93–104.

Clements, J. (1996). Transmitter time course in the synaptic cleft: its role in central synaptic transmission. Trends Neurosci. *19*, 163–171.

Clements, J., and Bekkers, J. (1997). Detection of spontaneous synaptic events with an optimally scaled template. Biophys. J. *73*, 220–229.

Craig, A.M., and Lichtman, J. (2001). Synapse formation and maturation. In Synapses, W.M. Cowan, T.C. Südhof, and C.F. Stevens, eds. (Baltimore, MD: Johns Hopkins University Press), pp. 571–612.

Cuttle, M.F., Tsujimoto, T., Forsythe, I.D., and Takahashi, T. (1998). Facilitation of the presynaptic calcium current at an auditory synapse in rat brainstem. J. Physiol. *512*, 723–729.

Diamond, J.S., and Jahr, C.E. (1997). Transporters buffer synaptically released glutamate on a submillisecond time scale. J. Neurosci. *17*, 4672–4687.

DiGregorio, D.A., Nusser, Z., and Silver, R.A. (2002). Spillover of glutamate onto synaptic AMPA receptors enhances fast transmission at a cerebellar synapse. Neuron *35*, 521–533.

Dobrunz, L.E. (2002). Release probability is regulated by the size of the readily releasable vesicle pool at excitatory synapses in hippocampus. Int. J. Dev. Neurosci. *20*, 225–236.

Dosemeci, A., Tao-Cheng, J.-H., Vinade, L., Winters, C.A., Pozzo-Miller, L., and Reese, T.S. (2001). Glutamate-induced transient modification of the postsynaptic density. Proc. Natl. Acad. Sci. USA *98*, 10428–10432.

Elmquist, D., and Quastel, D.M.J. (1965). A quantitative study of the end-plate potentials in isolated human muscle. J. Physiol. *178*, 505–529.

Fiala, J.C., and Harris, K.M. (2001). Cylindrical diameters method for calibrating section thickness in serial electron microscopy. J. Microsc. *202*, 468–472.

Forsythe, I.D. (1994). Direct patch recording from identified presynaptic terminals mediating glutamatergic EPSCs in the rat CNS, *in vitro*. J. Physiol. *479*, 381–387.

Forsythe, I.D., Tsujimoto, T., Barnes-Davies, M., Cuttle, M.F., and Takahashi, T. (1998). Inactivation of presynaptic calcium current contributes to synaptic depression at a fast central synapse. Neuron *20*, 797–807.

Geiger, J.R., and Jonas, P. (2000). Dynamic control of presynaptic Ca^{2+} inflow by fast-inactivating K^{+} channels in hippocampal mossy fiber boutons. Neuron *28*, 927–939.

Gillis, K.D. (1995). Techniques for membrane capacitance measurements. In Single Channel Recording, B. Sakmann and E. Neher, eds. (New York: Plenum Press), pp. 155–198.

Hanse, E., and Gustafsson, B. (2002). Release dependence to a paired stimulus at a synaptic release site with a small variable pool of immediately releasable vesicles. J. Neurosci. *22*, 4381–4387.

Harris, K.M., and Sultan, P. (1995). Variation in the number, location and size of synaptic vesicles provides an anatomical basis for the nonuniform probability of release at hippocampal CA1 synapses. Neuropharmacology *34*, 1387–1395.

Harris, K.M., Jensen, F.E., and Tsao, B. (1992). Three-dimensional structure of dendritic spines and synapses in rat hippocampus (CA1) at postnatal day 15 and adult ages: implications for the maturation of synaptic physiology and long-term potentiation. J. Neurosci. *12*, 2685–2705.

Hsia, A.Y., Malenka, R.C., and Nicoll, R.A. (1998). Development of excitatory circuitry in the hippocampus. J. Neurophysiol. *79*, 2013–2024.

Hsu, S.-F., and Jackson, M.B. (1996). Rapid exocytosis and endocytosis in nerve terminals of the rat posterior pituitary. J. Physiol. *494*, 539–553.

Ishikawa, T., and Takahashi, T. (2001). Mechanisms underlying presynaptic facilitatory effect of cyclothiazide at the calyx of Held of juvenile rats. J. Physiol. *533*, 423–431.

Iwasaki, S., and Takahashi, T. (1998). Developmental changes in calcium channel types mediating synaptic transmission in rat auditory brainstem. J. Physiol. *509*, 419–423.

Iwasaki, S., and Takahashi, T. (2001). Developmental regulation of transmitter release at the calyx of Held in rat auditory brainstem. J. Physiol. *534*, 861–871.

Jean-Baptiste, M., and Morest, D.K. (1975). Transneuronal changes of synaptic endings and nuclear chromatin in the trapezoid body following cochlear ablations in cats. J. Comp. Neurol. *162*, 111–134.

Joshi, I., and Wang, L.-Y. (2002). Developmental profiles of glutamate receptors and synaptic transmission at a single synapse in the mouse auditory brainstem. J. Physiol. *540*, 861–873.

Kandler, K., and Friauf, E. (1993). Pre- and postnatal development of efferent connections of the cochlear nucleus in the rat. J. Comp. Neurol. *328*, 161–184.

Kuwabara, N., DiCaprio, R.A., and Zook, J.M. (1991). Afferents to the medial nucleus of the trapezoid body and their collateral projections. J. Comp. Neurol. *314*, 684–706.

Lenn, N.J., and Reese, T.S. (1966). The fine structure of nerve endings in the nucleus of the trapezoid body and the ventral cochlear nucleus. Am. J. Anat. *118*, 375–390.

Lenzi, D., Crum, J., Ellisman, M.H., and Roberts, W.M. (2002). Depolarization redistributes synaptic membrane and creates a gradient of vesicles on the synaptic body at a ribbon synapse. Neuron *36*, 649–659.

Lin, J.-W., and Faber, D.S. (2002). Modulation of synaptic delay during synaptic plasticity. Trends Neurosci. *25*, 449–455.

Lohmann, C., and Friauf, E. (1996). Distribution of calcium-binding proteins parvalbumin and calretinin in the auditory brainstem of the adult and developing rats. J. Comp. Neurol. *367*, 90–109.

Lu, T., and Trussell, L. (2000). Inhibitory transmission mediated by asynchronous transmitter release. Neuron *26*, 683–694.

Martin, A.R., and Pilar, G. (1964). Presynaptic and postsynaptic events during posttetanic potentiation and facilitation in the avian ciliary ganglion. J. Physiol. *175*, 17–30.

Meinrenken, C.J., Borst, J.G.G., and Sakmann, B. (2002). Calcium secretion coupling at the calyx of Held governed by nonuniform channel-vesicle topography. J. Neurosci. *22*, 1648–1667.

Meyer, A.C., Neher, E., and Schneggenburger, R. (2001). Estimation of quantal size and number of functional active zones at the calyx of Held synapse by nonstationary EPSC variance analysis. J. Neurosci. *21*, 7889–7900.

Mintz, I.M., Sabatini, B.L., and Regehr, W.G. (1995). Calcium control of transmitter release at a cerebellar synapse. Neuron *15*, 675–688.

Morest, D.K. (1968). The growth of synaptic endings in the mammalian brain: a study of the calyces of the trapezoid body. Z. Anat. Entwicklungsgesch *127*, 201–220.

Mozhayeva, M.G., Sara, Y., Liu, X., and Kavalali, E.T. (2002). Development of vesicle pools during maturation of hippocampal synapses. J. Neurosci. *22*, 654–665.

Murthy, V.N., Schikorski, T., Stevens, C.F., and Zhu, Y. (2001). Inactivity produces increases in neurotransmitter release and synapse size. Neuron *32*, 673–682.

Nicol, M.J., and Walmsley, B. (2002). Ultrastructural basis of synaptic transmission between endbulbs of Held and bushy cells in the rat cochlear nucleus. J. Physiol. *539*, 713–723.

Oleskevich, S., and Walmsley, B. (2002). Synaptic transmission in the auditory brainstem of normal and congenitally deaf mice. J. Physiol. *540*, 447–455.

Oertner, T.G., Sabatini, B.L., Nimchinsky, E.A., and Svoboda, K. (2002). Facilitation at single synapses probed with optical quantal analysis. Nat. Neurosci. *5*, 657–664.

Otis, T., Wu, Y.C., and Trussell, L.O. (1996). Delayed clearance of transmitter and the role of glutamate transporters at synapses with multiple release sites. J. Neurosci. *16*, 1634–1644.

Parks, T.N. (2000). The AMPA receptors of auditory neurons. Hear. Res. *147*, 77–91.

Partin, K.M., Patneau, D.K., and Mayer, M.L. (1994). Cyclothiazide differentially modulates desensitization of AMPA receptor splice variants. Mol. Pharmacol. *46*, 129–138.

Redd, E.E., Pongstaporn, T., and Ryugo, D.K. (2000). The effects of congenital deafness on auditory nerve synapses and globular bushy cells in cats. Hear. Res. *147*, 160–174.

Renger, J.J., Egles, C., and Liu, G. (2001). A developmental switch in neurotransmitter flux enhances synaptic efficacy by affecting AMPA receptor activation. Neuron *29*, 469–484.

Roos, J., and Kelly, R.B. (1999). The endocytic machinery in nerve terminals surrounds sites of exocytosis. Curr. Biol. *9*, 1411–1414.

Rosenmund, C., Clements, J.D., and Westbrook, G. (1993). Nonuniform probability of glutamate release at a hippocampal synapse. Science *262*, 754–757.

Rossi, D.J., Alford, S., Mugnaini, E., and Slater, N.T. (1995). Properties of transmission at a giant glutamatergic synapse in cerebellum: the mossy fiber-unipolar brush cell synapse. J. Neurophysiol. *74*, 24–42.

Rowland, K.C., Irby, N.K., and Spirou, G.A. (2000). Specialized synapse-associated structures within the calyx of Held. J. Neurosci. *20*, 9135–9144.

Ryugo, D.K., Wu, M.M., and Pongstaporn, T. (1996). Activity-related features of synapse morphology: a study of endbulbs of Held. J. Comp. Neurol. *365*, 141–158.

Sakaba, T., and Neher, E. (2001). Quantitative relationship between transmitter release and calcium current at the calyx of Held synapse. J. Neurosci. *21*, 462–476.

Sätzler, K., Söhl, L.F., Bollmann, J.H., Borst, J.G.G., Frotscher, M., Sakmann, B., and Lübke, J.H.R. (2002). Three dimensional reconstruction of a calyx of Held and its postsynaptic principal neuron in the MNTB. J. Neurosci., in press.

Scheuss, V., Schneggenburger, R., and Neher, E. (2002). Separation of presynaptic and postsynaptic contributions to depression by covariance analysis of successive EPSCs at the calyx of Held synapse. J. Neurosci. *22*, 728–739.

Schikorski, T., and Stevens, C.F. (1997). Quantitative ultrastructural

analysis of hippocampal excitatory synapses. J. Neurosci. *17*, 5858–5867.

Schneggenburger, R., and Neher, E. (2000). Intracellular calcium dependence of transmitter release rates at a fast central synapse. Nature *406*, 889–893.

Schneggenburger, R., Meyer, A.C., and Neher, E. (1999). Released fraction and total size of a pool of immediately available transmitter quanta at a calyx synapse. Neuron *23*, 399–409.

Sekiguchi, M., Fleck, M.W., Mayer, M.L., Takeo, J., Chiba, Y., Yamashita, S., and Wada, K. (1997). A novel allosteric potentiator of AMPA receptors: 4-2-(phenylsulfonylamino)ethylthio-2,6-difluoro-phenoxyaceta mide. J. Neurosci. *17*, 5760–5771.

Silver, R.A., Momiyama, A., and Cull-Candy, S.G. (1998). Locus of frequency-dependent depression identified with multiple-probability fluctuation analysis at rat climbing fibre-Purkinje cell synapses. J. Physiol. *510*, 881–902.

Smith, P.H., Joris, P.X., Carney, L.H., and Yin, T.C. (1991). Projections of physiologically characterized globular bushy cell axons from the cochlear nucleus of the cat. J. Comp. Neurol. *304*, 387–407.

Smith, P.H., Joris, P.X., and Yin, T.C. (1998). Anatomy and physiology of principal cells of the medial nucleus of the trapezoid body (MNTB) of the cat. J. Neurophysiol. *79*, 3127–3142.

Sun, J.-Y., and Wu, L.-G. (2001). Fast kinetics of exocytosis revealed by simultaneous measurements of presynaptic capacitance and postsynaptic currents at a central synapse. Neuron *30*, 171–182.

Sun, J.-Y., Wu, X.-S., and Wu, L.-G. (2002). Single and multiple vesicle fusion induce different rates of endocytosis at a central synapse. Nature *417*, 555–559.

Taschenberger, H., and von Gersdorff, H. (2000). Fine-tuning an auditory synapse for speed and fidelity: developmental changes in presynaptic waveform, EPSC kinetics, and synaptic plasticity. J. Neurosci. *20*, 9162–9173.

Tatsuoka, H., and Reese, T.S. (1989). New structural features of synapses in the anteroventral cochlear nucleus prepared by direct freezing and freeze-substitution. J. Comp. Neurol. *290*, 343–357.

Teng, H., and Wilkinson, R.S. (2000). Clathrin-mediated endocytosis near active zones in snake motor boutons. J. Neurosci. *20*, 7986–7993.

Trussell, L.O., Zhang, S., and Raman, I.M. (1993). Desensitization of AMPA receptors upon multiquantal neurotransmitter release. Neuron *10*, 1185–1196.

Vaughn, J.E. (1989). Fine structure of synaptogenesis in the vertebrate central nervous system. Synapse *3*, 255–285.

von Gersdorff, H., Vardi, E., Matthews, G., and Sterling, P. (1996). Evidence that vesicles on the synaptic ribbon of retinal bipolar neurons can be rapidly released. Neuron *16*, 1221–1227.

Wadiche, J.I., and Jahr, C.E. (2001). Multivesicular release at climbing fiber-Purkinje cell synapses. Neuron *32*, 301–313.

Wang, L.Y., and Kaczmarek, L.K. (1998). High-frequency firing helps replenish the readily releasable pool of synaptic vesicles. Nature *394*, 384–388.

Wu, L.-G., and Borst, J.G.G. (1999). The reduced release probability of releasable vesicles during recovery from short-term synaptic depression. Neuron *23*, 821–832.

Wu, S.H., and Oertel, D. (1987). Maturation of synapses and electrical properties of cells in the cochlear nuclei. Hear. Res. *30*, 99–110.

Wu, L.-G., Westenbroek, R.E., Borst, J.G.G., Catterall, W.A., and Sakmann, B. (1999). Calcium channel types with distinct presynaptic localization couple differentially to transmitter release in single calyx-type synapses. J. Neurosci. *19*, 726–736.

Xu-Friedman, M., Harris, K.M., and Regehr, W.G. (2001). Three-dimensional comparison of ultrastructural characteristics at depressing and facilitating synapses onto cerebellar Purkinje cells. J. Neurosci. *21*, 6666–6672.